이학박사 학위논문

Study on chiral domain wall in ultra-thin films:

Tailoring of spin orbit torque and Dzyaloshinskii-Moriya interaction

수직 이방성 자성초박막의 나선 자구벽에 관한 연구:

스핀궤도 토크와 Dzyaloshinskii−Moria 상호작용의 소자 구동원리

2015년 8월

서울대학교 대학원

물리천문학부

조 정 구

Study on chiral domain wall in ultra-thin films:

Tailoring of spin orbit torque and Dzyaloshinskii-Moriya interaction

수직 이방성 자성초박막의 나선 자구벽에 관한 연구:

스핀궤도 토크와 Dzyaloshinskii–Moria 상호작용의 소자 구동원리

지도교수 최석봉

이 논문을 이학박사 학위논문으로 제출함

2015년 8월

서울대학교 대학원

물리천문학부

조 정 구

조정구의 이학박사 학위논문을 인준함

2015년 8월

위 원 장	강 병 남	(인)
부위원장	최 석 봉	(인)
위 원	박 윤	(인)
위 원	홍 성 철	(인)
위 원	류 광 수	(인)

Study on chiral domain wall in ultra-thin films:

Tailoring of spin orbit torque and Dzyaloshinskii-Moria interaction

Cheong-Gu Cho

Supervised by
Professor Sug-Bong Choe

A Dissertation in Physics

Submitted to the Faculties of
Seoul National University
in Partial Fulfillment of the Requirements for the Degree of
Doctor of Philosophy

August 2015

Department of Physics and Astronomy
The Graduate College of Natural Sciences
Seoul National University

Abstract

As the circuit wire width of DRAM used today got near to the scale of 10nm which is the physical lower limit, there has aroused various problems regarding cost efficiency, structure-design and so on. To overcome these new challenges, the interest in new-generation memory device has increased drastically. The magnetic memory device using spintronics have proven itself to be one of the promising candidates, as it excels in solving various problems regarding writing/reading time, endurance, non-volatility, power consumption and so on. This is the reason why spintronics is being studied hard both industrially and scholarly.

This paper focuses on solving physical problems hindering the mass production of Spin torque device. Those problems are as listed: 1)High speed, 2)Read-Write reliability, 3)High density & low energy consumption. Some new interesting physical phenomena such as spin orbit torque(SOT) and Dzyaloshinskii-Moriya interaction(DMI) have been discovered and studied in the course of time.

In chapter 1, the start and expected future of new memory device using spintronics will be introduced. Recently various kinds of new-generation memory have suggested. We will specify the unique properties of spintronics memory device. Device using spin-torque has been studied in 2 ways which will be introduced in details. First the STT-MRAM with current flowing through 2 magnetic layers separated by nonmagnetic layer, and second the SOT-MRAM with current flowing in the plane of domain walls will be discussed.

In chapter 2, we discuss the ultrathin film with perpendicular magnetic anisotropy that minimizes the influence of sputtering defects that hinder the domain wall movement. We developed various manufacturing methods with sputtering system and they will be discussed in detail here. To measure the width of the film layers, we used XRT/AFM to analyze the structure of ultrathin film. Set of films with structure modification by annealing effect have been produced. Measuring these films led to the

empirical correlation between structure property and magnetic property.

In chapter 3, the Gilbert damping constant is the main subject. This is related with the high performance of spin torque device. The definition and significance of Gilbert damping is explained. To optimize this constant, we studied various related magnetic properties and finally achieved the method to control it via structure tailoring.

In chapter 4, we investigate the SOT and DMI in Co films sandwiched by various 3d, 4d, and 5d transition metals. Recently, it has been found that the efficiency of domain-wall motion driven by current can be largely enhanced by the SOT combined with the DMI. It is therefore important to analyze the sign and magnitude of the DMI and SOT to understand their physical origin as well as to achieve memory and logic devices. In this study, we report the DMI and SOT of various metallic ferromagnetic films, of which the structures are Ta(5 nm)/Pt(2.5 nm)/Co(0.6 nm)/X(5nm) films with various choice of X by Ti(3d), Cu(3d), Ru(4d), Pd(4d), Ta(5d), W(5d), Au(5d), and Mg. The sign and magnitude of the DMI and SOT are then measured from the asymmetric domain-wall expansion and ω-2ω measurement method, respectively. The overall trend depending on the material combination will be discussed.

In chapter 5, we control the SOT and DMI by use of Mg insertion to Pt/Co/Pt structure. The Mg insertion layer thickness dependence of DMI sign and magnitude was measured by asymmetric DW expansion method. From the measured dependence, it has been shown that the DMI field can be controlled via film structure tailoring.

In chapter 6, the whole dissertation is concluded. The physical origin of SOT and DMI has been studied scientifically. The DMI and SOT of various films have been measured and classified in hierarchical manner. The material design rule from it has suggested the method to tailor spin torque devices. This hierarchical approach to tailor spin torque memory devices is becoming a stepping stone to the future of nanomagnetism.

Keywords: Magnetic domain, domain wall, spin torque device, spin transfer torque, spin orbit torque, next generation magnetic memory, perpendicular magnetic anisotropy, Dzyaloshinskii-Moriya interaction, chiral domain wall

Student number: 2010-30116

Table of Contents

List of Figures

Chapter 1

General introduction

1.1 Spintronics: magnetic memories with a spin

Today's memory device needs to be mobile and in a meantime provide terabytes storage for computational system. The memory industries have been on competition to develop better devices with these adjectives like -high density, non-volatile, high performance for storing and dealing an avalanche of digital data. The memory hierarchy are mainly developed for this purpose: Hard disk drive (HDD), dynamic random access memory (DRAM) and flash memory.

The HDD for non-volatile data storage already achieved a terabyte process. It however showed a slow data access (a few milliseconds) because of its read/write procedure involve moving mechanical parts [1]. DRAM, on the other hand, has a nanosecond time scale for read/write due to its solid-state electronic device. But DRAM has its own cons too. Every data process in DRAM are volatile information due to its capacitor structure [2]. Flash memory is getting more interest with the growth of mobile applications. Flash memory is a non-volatile memory and has high density data storage, but it has a relatively slow data process and low-endurance [2]

Spin torque device has been intensively studied over last decades due to its promising application toward memories and logic devices with high-density storage and low-energy consumption. The data is stored in the

magnetization of nanomagnet in spin torque devices. This is a solid stated memory which is available to read/write electrically. This is an advantage when it comes to the integration of magnetic devices with semiconductor chip. Due to the data storage into the magnetization, It has no energy cost for maintaining an information and has a non-volatile property

(a) (b)

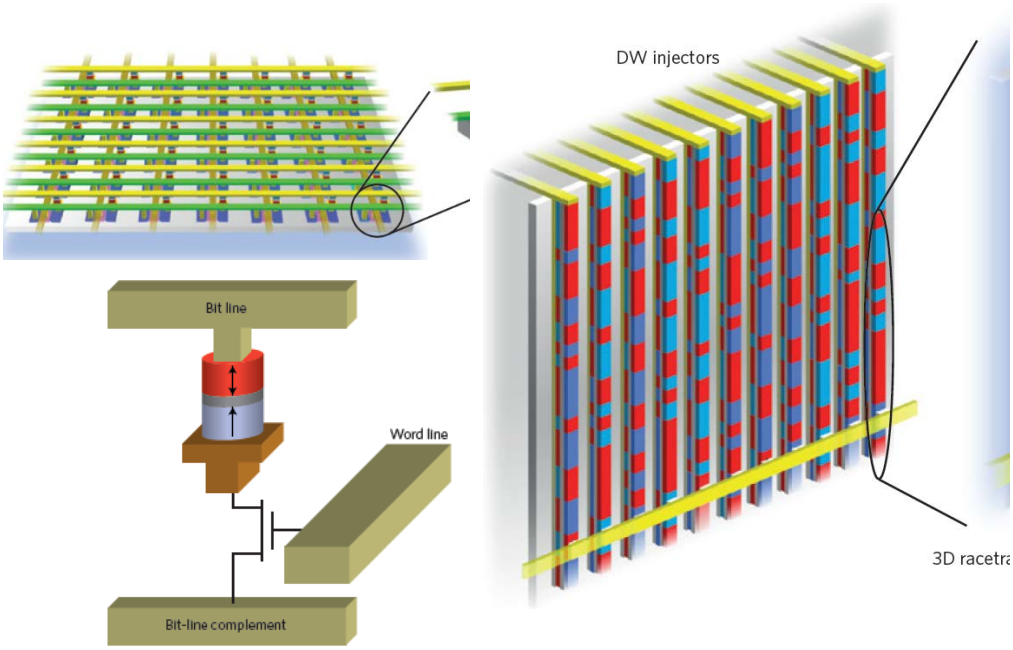

Figure 1.1 (a)Schematic illustration of STT-MRAM, (b)DW device i.e racetrack memory. Illustraion from ref. 2, 7

In recent studies approached spin torque devices in two distinct ways. Spin-transfer-torque magnetic random access memory (STT-MRAM) is one. STT-MRAM is a nano-pillar structure which have two ferromagnetic

layers divided by non-ferromagnetic layer. Each magnetization within the nano-pillar is controlled by incident spin current. This process becomes the read/write step for data storage. Domain-wall (DW) device is a two. DW device consists of nano-wire that has multi-DWs on it which are controlled by incident spin current. Figure 1.1 shows a schematics of STT-MRAM and DW device respectively [2, 7]. Compared to other candidates of next generation memory such as Phase change memory (PCM), resistive random access memory(RRAM), conductive bridge random access memory(CBRAM) and so on, STT-MRAM transcend in endurance cycling and speed. Its low resistance ratio however requires a memory cell architecture and that limits its memory density. [6][Fig1. 2.]

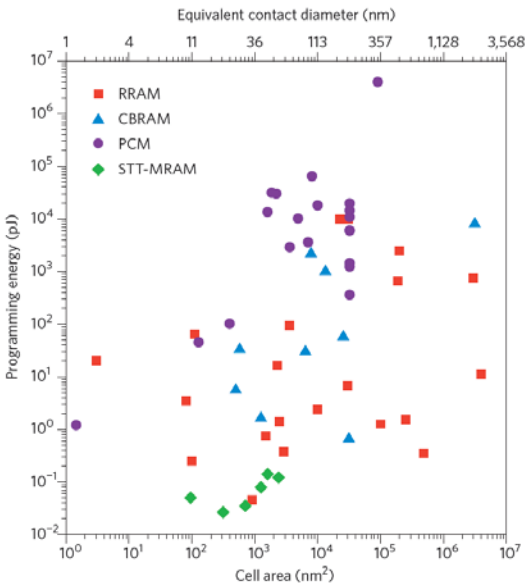

Figure 1.2. A comparison of key attributes (write energy versus device size) for various emerging non-volatile memories. Data form ref. 6

To realize a spin torque device, we should understand a physics under

STT. STT has been theoretically proposed by Slonczewski [3, 4, 5]. As the spin angular momentum of incident conduction electron transfers to the local magnetization, the magnetization changes. This is called s-d exchange interaction (interaction between 3d electron of local magnetization and incident 4s electron) It is explained by Landau-Lifshitz-Gilbert(LLG) equation like below.

$$\frac{\partial \overrightarrow{M(t)}}{\partial t} = \underbrace{-\gamma_0 \overrightarrow{M} \times \overrightarrow{H_{eff}}}_{\text{1) Precession term}} + \underbrace{\frac{\alpha}{M_S} \overrightarrow{M} \times \frac{\partial \overrightarrow{M(t)}}{\partial t}}_{\text{2) Gilbert damping term}} - \underbrace{\frac{b_J}{M_s^2} \overrightarrow{M} \times (\overrightarrow{M} \times \frac{\partial \overrightarrow{M}}{\partial x})}_{\text{3) Adiabatic term}} \underbrace{- \frac{c_J}{M_s} \overrightarrow{M} \times \frac{\partial \overrightarrow{M}}{\partial x}}_{\text{4) Non-adabatic term}} \quad (1.1)$$

1) Magnetization M aligns itself to external effective field H_{eff} direction while precession happens in the course. 2) Gilbert damping term arises from energy dissipation. 3) Adiabatic term that represents aligning of conduction electron into the local magnetization 4) Non-adiabatic term that represents aligning of local magnetization due to spin angular momentum transfer by conduction electron. Understanding these terms and further physics of STT provides a radical clue for engineering spin torque devices to have the high speed, the read-write reliability, the high density, and the low energy consumption.

Reference

[1] Editorial, *Nature Nano*tech. 10, 185(2015)

[2] Andrew D. Kent and Daniel C. Worledge, *Nature Nanotech*. 10, 187(2015)

[3] Slonczewski, J. C. *Phys. Rev. B* 39, 6995–7002 (1989).

[4] Slonczewski, J. C. *J. Magn. Magn. Mater*. 159, L1–L7 (1996).

[5] Berger, L. *Phys. Rev. B* 54, 9353–9358 (1996).

[6] H.-S. Philip Wong and Sayeef Salahuddin, *Nature Naonotech*. 10, 191(2015)

[7] Stuart Parkin and See-Hun Yang, *Nature Naonotech.* 10, 197(2015)

[8] Mahdi Jamali et al., *Phys. Rev. Lett* 111, 246602 (2013).

[9] I. M. Miron et al., *Nature* 476, 189 (2011).

[10] S.-G. Je et al., *Phys. Rev. B* 88, 214401 (2014)

[11] H. L. Wang et al., *Phys. Rev. Lett*. 112,197201 (2014)

[12] A. V. Khvalkovskiy et al., *Phys. Rev. B* 87, 020402 (2013)

[13] Weiss, *P. Campt. Rend.,* 143, 1136 (1906)

[14] Weiss, *P. J.Phys*., 6, 661(1907)

[15] Landau, L. D. and Lifschitz, *E.M. physic Z. sowjetunion* 8, 153 (1935)

[16] Bloch. F., *Phyzik* 74, 295 (1932)

[17] David Jiles., *Introduction to magnetism a magnetic materials*, chapter 7. Page127

[18] S. Lemerle et al. *Phys. Rev. Lett.* 80, 849 (1998).

[19] P. Chauve et al.. *Phys.Rev. B* 62, 6241 (2000).

[20] J. Ryu et al.. *Phys. Rev. B* 84, 075469 (2011).

[21] K.-J. Kim et al*Nature* (London) 458, 740 (2009).

[22] F. Cayssol et al. *Phys. Rev. Lett*. 92, 107202 (2004).

[23] P. J. Metaxas et al. *Phys. Rev. Lett.* 99, 217208 (2007)

Chapter 2

Evolution of sample fabrication

In this chapter, we are searching for best PMA films. In DW motion in PMA films, there is a disorder by processing of deposition. It is, therefore, reducing a disorder is a critical issue. We approach a film morphology for reducing disorder, which made a DW propagate easily. For this study, we manufactured ultra-high vacuum sputtering systems. Interface roughness and sharpness of films are controlled by deposition condition, which is related with microstructural defect reducing. We are then, search a various material with different spin Hall angle/sign and with different crystal structure for optimal structure of SOT and DMI experiment.

Section 2.1 describes a physics of PMA and optimal deposition condition. Sputtering systems which we manufactured are introduced. Section 2.2 report a sample for STT experiment. Section 2.3 report a sample for Gilbert damping constant. Section 2.4 describe a sample for SOT and DMI. We will discuss a magnetic properties of each experiment..

2.1 Sample fabrication and experimental setup

2.1.1 Manufacturing a sputtering system for deposition

Since discovery of PMA [1,2], direct imaging of DW in PMA films has been a subject of great interest for its technological applications. Origin of Co PMA is fully understanding as interface orbital hybridization due to a spin orbit interaction [3, 6~8]. The layer interface between Co layer and other metals should controlled during a deposition process. For the growth a proper films, we design and manufacture the sputtering systems. Figure 2.1 describe an in-situ sputtering system. This system is composed by 4 part: i) Metal deposition chamber: Base pressure is under 3.0 x 10^{9} torr with 7 guns. A deposition controlled by programmable computer which error accuracy of deposition rate is 0.5%. Each deposition use a DC power supply with constant Watt controlled. ii) Oxidation deposition chamber: Base pressure is under 5.0 x 10^{8} torr with 3 guns. It also controlled by programmable computer which error accuracy of deposition rate is 0.5%. Each deposition use a RF power supply with a reflection power under 1% accuracy. iii) Elevation chamber: Base pressure under 5.0 x 10^{8} torr with 8 chuck. This chamber make a sample transfer in high vacuum state. iv) Ion-milling chamber: Base pressuere under 5.0 x 10^{7} torr. Milling source is used a Kaufman method [9]. A milling rate is about ~5nm/min milling rate for Pt films.

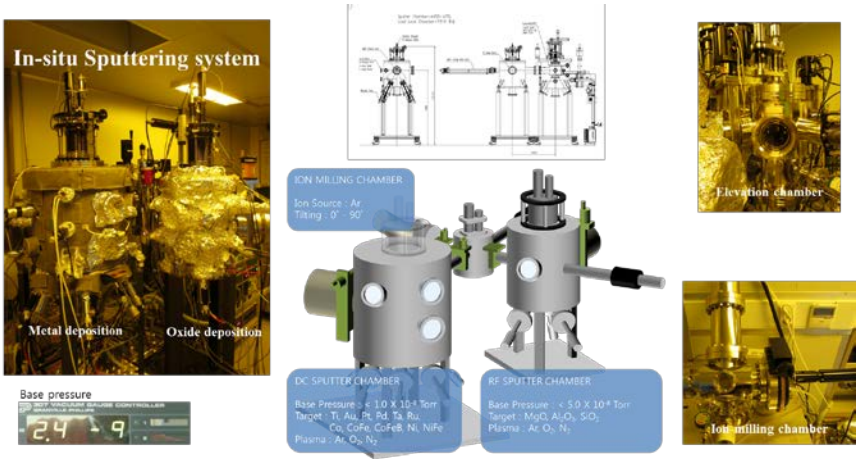

Figure 2.1 Schematic picture of in-situ sputtering system.

From this home-made in-situ sputtering system, we grow the Co ultra-thin films with PMA. The DW patterns of various film are observed by a magneto-optical Kerr microscope as follow figure 2.2.

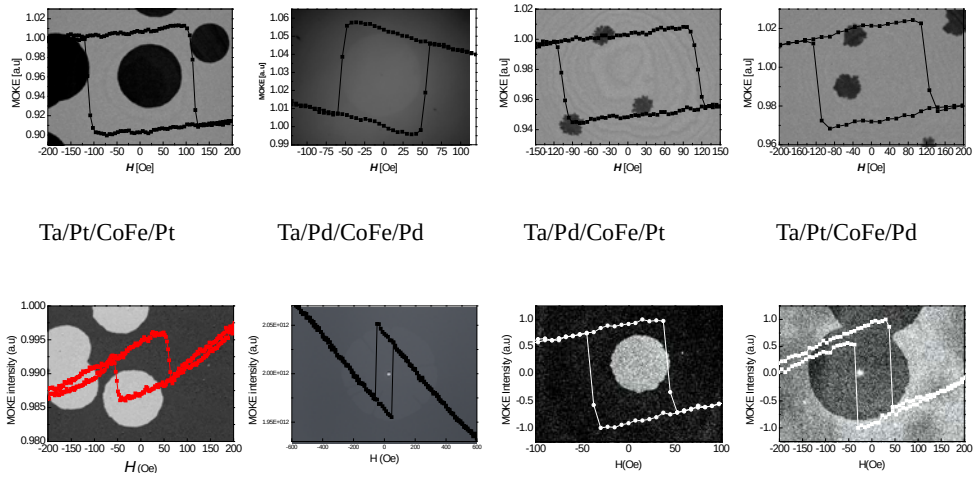

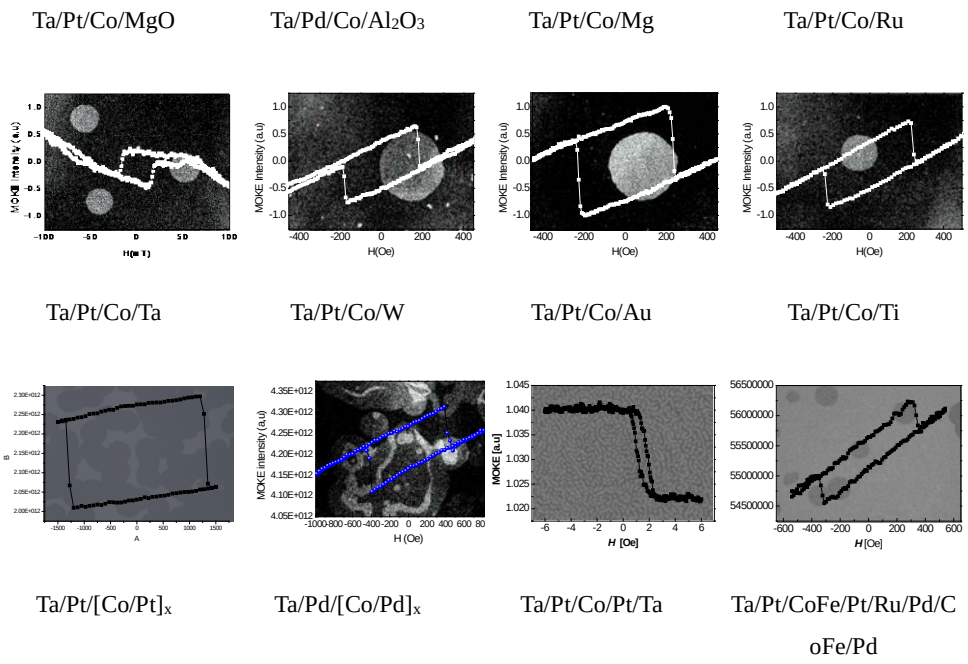

Figure 2.2 The DW patterns of various Co films with PMA

2.1.2 Development of Co thin film with optimized defect structure

The DW in PMA films have a different pattern which is related on reversal process [10~13]. There is a three distinct phase of DW patterns: Wall motion, dendrite growth and nucleation. The large DW motion have a many opportunity in spin torque application due to its low disorder density. It is, therefore, a purpose of this section to make a clear circular domain wall.

To control a DW reversal patterns, we have to understand a magneto static energy contribution [14]. The large magneto static layer make a DW reversal pattern to large domain wall phase. From the previous reports [4, 5], large domains are observed as decreasing ferromagnetic layer thickness with

strong PMA. It is therefore decreasing a Co thickness is crucial process when we make a PMA films. Section 2.2 will be discuss about clear circular large domain wall in Pt 2.5 nm / Co 0.3 nm / Pt 1.5 nm PMA films.

Microstructural disorder which is origin of pinning site should be reduced for DW propagation. For optimizing a morphology of ultra-thin films, we reducing a deposition rate under monolayer level (<0.15Å/sec) adjusting with high Ar pressure (3 mtorr) and low sputtering power (~10W). The sputtering condition is not only parameter for reducing a microstructural disorder, but crystalline of layer interface also crucial parameter when we fabricate. From Bruno's theory [3], the interface of Pt layer which is well growth with its natural prefer orientation fcc(111) enhance a spin orbit coupling for orbital hybridization on interface. This is because involving with magnetocrystralline anisotropy. We should consider about crystalline state when we deposit a Pt layers. For this optimization, we control a crystalline state using Ar flow rate. Figure 2.3 clearly shown a dependence of Pt and Co layer crystalline in Pt 5 nm / Co 30 nm / Pt 2nm with respect to Ar flow rate. In Pt 2.5nm / Co 0.3 nm / Pt 1.5 nm with different Ar flow, out of plane loop is also distinct shape with respect to Ar flow rate. We choose an Ar flow rate under 10 sccm for strong PMA.

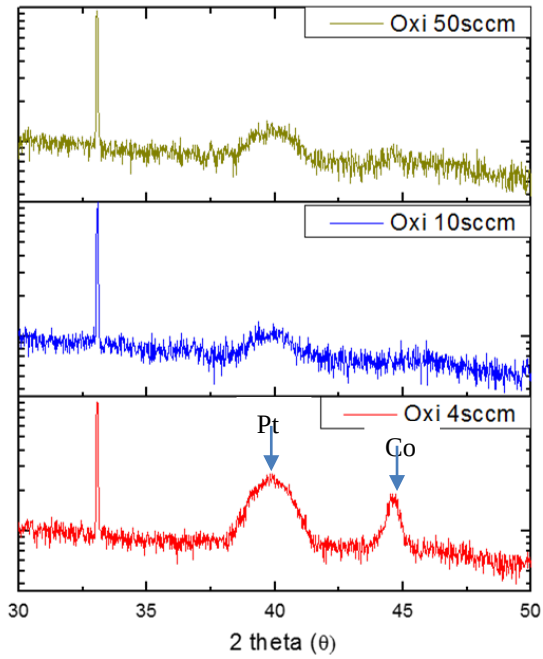

Figure 2.3 XRD result of Pt 5nm / Co 30 nm / Pt 2nm. The crystalline of Pt and Co are dramatic change with decreasing Ar flow rate.

2.2 Fabrication process

Fabrication step are shown in figure 2.4. Nano-/Micro-wire are patterned by using E-beam/Photo lithography and ion-milling. E-beam/Photo lithography is for making a ferromagnetic nano-/micro-wire with electric pad. Ion-milling steps are divide as 3 angles(15, 30, 75°) for control a roughness of wire edge. For controlling a magnetization by means of incident current, electrode are deposited on ferromagnetic wires.

Detail process are shown as following step

(i) Cleaning substrate

Si(100) 625 μm /SiO_2 100 nm is used for substrate. We remove a particle and organic contamination before a deposition. First, we use a Chloroform liquid of T=100 °C for 20 min to remove an organic contamination. The substrate are then cleaned by Acetone and Methanol for 10min and 5min in ultrasonic cleaner at room temperature, respectively. The substrate is the rinsed in DI-water and dried by N_2 gas. In order to remove remaining H_2O, it is baked on hot plate for 1minute at 100°C or dried out using vacuum chamber.

(ii) E-beam lithography and photolithography

We use a positive and negative E-beam resist(ER). Positive tone ER by means of double-layer of PMMA 950K A2 and 495K A4 as an inter-connected wire structure. Both resist coating condition is the same as 1000rpm for first 10sec and 4000 rpm for continuous 50 sec, respectively. The baking conditions are 150°C for PMMA 950K A2 and 180°C for PMMA 495K The negative tone ER, which is used ma-N2403, is adapt for fin relosution (~5nm).The coating condition is same as positive tone. The coating condition of ER is 1500rpm for first 0.5sec and 4000rpm for continuous 30sec. The baking conintion is 90°C for 60 sec. The developer for ER are used MIBK : IPA(3:1). E-beam lithography system, as it called JBX600FS/E, support a 100eV of Gaussian beam which is cover a 500 um * 500 um. The developer for positive ER are used MIBK : IPA(3:1). We use a field electron emission sources, such as W/ZrO_2 for lower energy density and enhanced intensity.

The photolithography process is used AZ5214E and DNR as a

photo-resist. The AZ5214 as a positive resist, we cover a PR with 500 rpm for the first, after then continuous coating with 4000 rpm with 60sec. The baking condition is 95°C for 7 min in the oven. The negative tone, DNR, is 100 to 500 rpm gradually increased during first 5sec, after then continuous 5000 rpm with 60 sec. Pre-baking is 110°C in hot plate 100 sec, after expose, post-bake 110°C in hot plate 100 sec. The photolithography system is used MA6 (SUSS) with 350W UV lamp. The intensity is 8mJ/cm^2.

(iii) Milling and lift-off process

The milling process is designed for reducing an edge roughness and etching a few Å depth sensitivity. We have a rotational stage which could tilt angle 10° to 90° from the film normal direction. Milling angle is chosen at 3 part (15, 30, 75°) because re-sputtered particle is attached in single angle. We use a ion source with a Kaufman method that control the acceleration voltage 0 to 250V, which is advanced for depth sensitivity. The lift-off process is used a double-layered pattern and under-cut structure. In single layer patterned lift-off process, it usually cause a “rabbit-ear” shape which make an edge roughness problem. We enhance an edge roughness without rabbit-ear shape using a double-layered resist and under-cut shaped resist.

2.3 Sample fabrication for experiment of spin transfer torque

2.3.1 Pt/Co/Pt structure

Previous report [15], Ta 5nm / Pt 2.5 nm / Co 0.3 nm / Pt 1.5 nm is best film structure for STT experiment. This films have extremely low extrinsic pinning site, which is easy to propagate DW by STT. This films have a large DW motion by small external field. First we check the DW pattern, then check a velocity of DW for confirming a creep law. Figure 2.4.(a) clearly shown a DW pattern as large DW motion. Figure 2.4.(b) shown a DW velocity which following a creep law. This DW propagation is detected under even less than 1mT. This structure generally used in STT experiment.

(a)

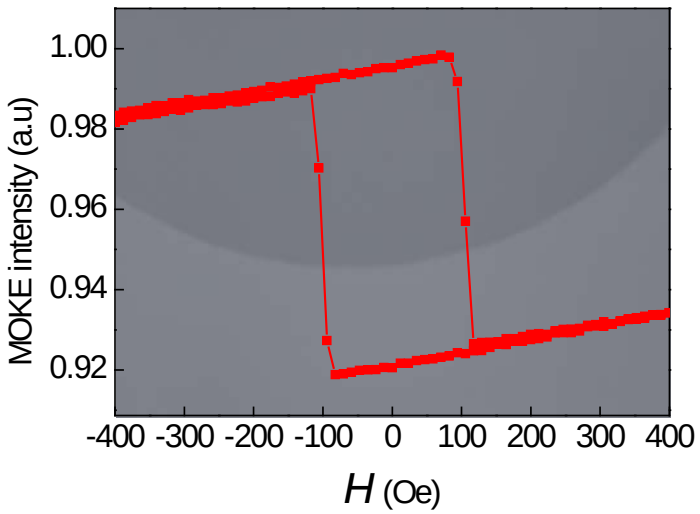

(b)

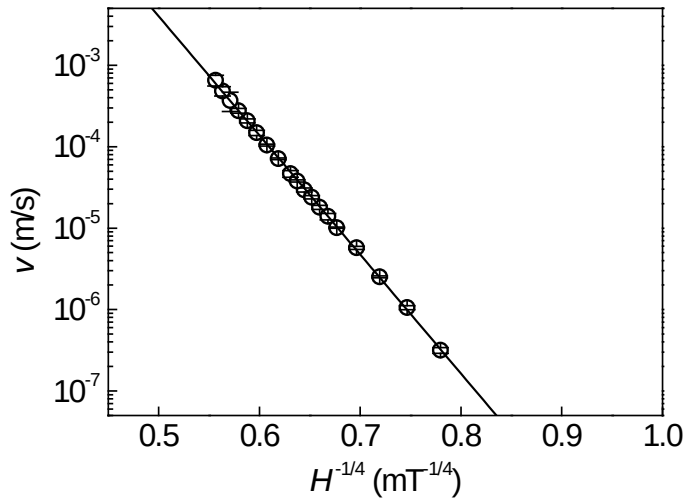

Figure 2. 4 (a) Large circular DW motion which propagate easily because of its low microstructural disorder (b) DW velocity follow the creep law.

2.3.2 Pd/Co/Pd structure

Current induced DW motion is firstly developed in Pt/Co/Pt structure [15]. It is easy to adapt an experiment of STT because Pd/Co/Pd PMA films have also strong PMA. The Pd layer, however, have a different electrical properties which means the transport of electron is not the same case of Pt/Co/Pt [16]. For STT experiment, we control a deposition condition which reducing a microstructural pinning. Figure 2.5 shown a clearly circular large DW motion. This films are fabricated on ~mm size for 2 dimensional effect of STT [17, 18, 19]. We choose a Pd 2.5nm / Co 0.3 nm / Pd 2nm with optimized structure.

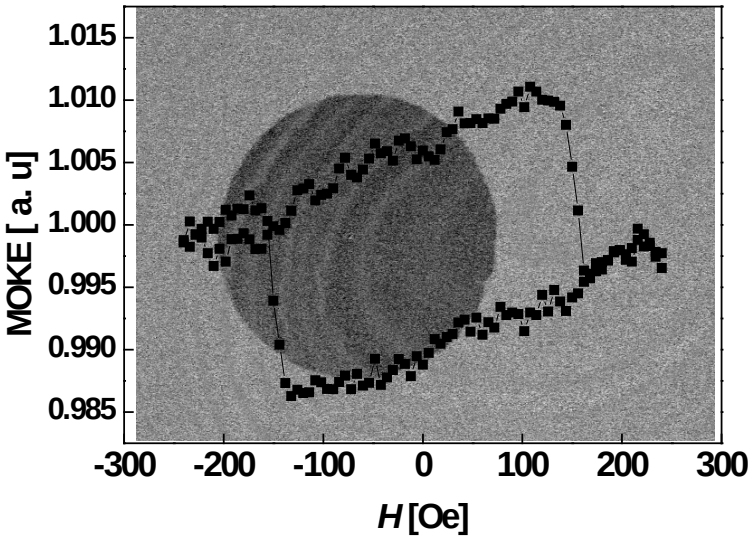

(a)

(b)

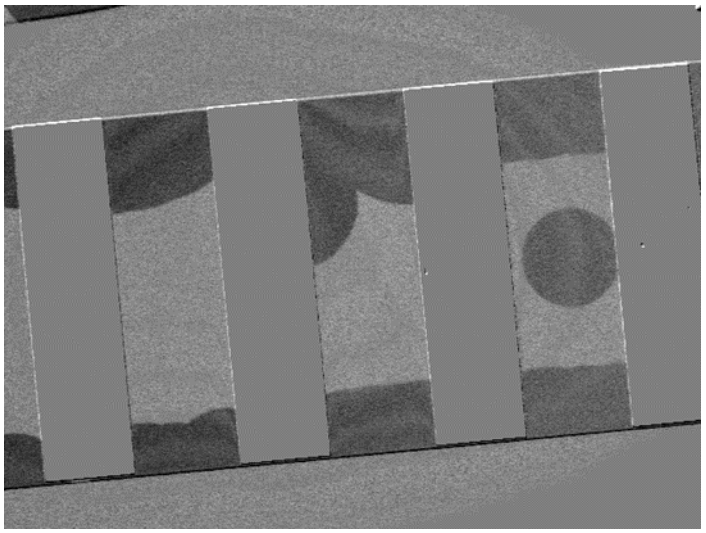

Figure 2.5 (a) Large circular DW in Ta 5nm/ Pd 2.5nm/ Co 0.3nm/ Pd 2nm structure (b) 1mm wire sample for 2D STT experiment which fabricated with ion milling.

2.3.3 Pt/Co/Oxide structure

In recent study, Heavy metal / Ferromagnetic metal / Oxide heterostructure is great interest due to its enhancement of SOT efficiency and observation of DMI. It is, however, not easy to fabricate the PMA films with large circular DW. Engineering an interface between ferromagnetic metal and oxide is complicated due to hybridization of orbital which is prefer a selective condition [20]. We examine the PMA films with various Co thickness in Pt/Co/Oxide structure (Oxide/Co/Pt structure also checked). The MOKE microscope observed DW pattern and propagation properties [21, Figure 2.6]. The anisotropy field was determined by extraordinary Hall torque measurement [29, Figure 2.9]. The DW pattern is affected by Co thickness because of its magneto static energy as follow figure 2.6. The thickness of Pt and Ta or oxide layer, furthermore, is determine a coercive field and distribution of nucleation cite due to disorders during a deposition. Figure 2.7 clearly shown a optimization thickness of Ta/Pt/Co/Oxide(MgO) films. The Annealing temperature and time is involving oxide PMA films development. Co 3d orbital hybridized with O 2p orbital which determine the band filling. It cause a interfacial anisotropy which is extremely sensitive to interface of Co [22-24]. We control the interface state using optimization of annealing temperature and time, as follow figure 2.8.

Figure 2.9 shown the anisotropy depend on Co thickness with various oxide PMA films. The Anisotropy field H_k has a maximum value for t_{Co}~1 nm irrespective to the oxide layers. These explain that the measurement technique using extraordinary Hall effect has a high accuracy when determine the

anisotropy field H_k in PMA sample.

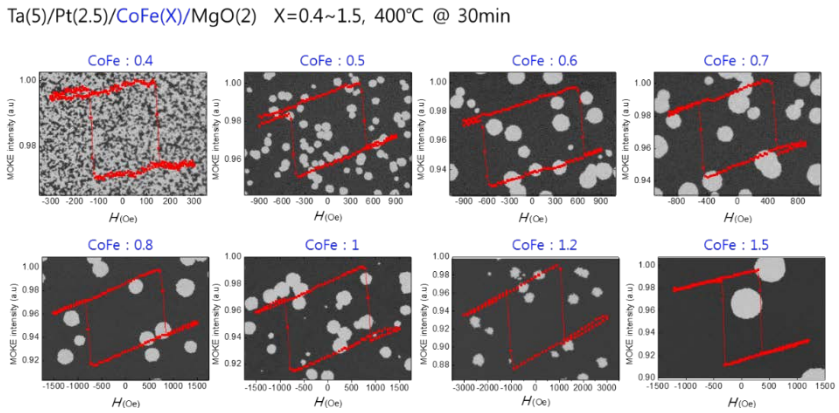

Figure 2.6 Ta/Pt/CoFe/MgO PMA films optimization using CoFe thickness variation.

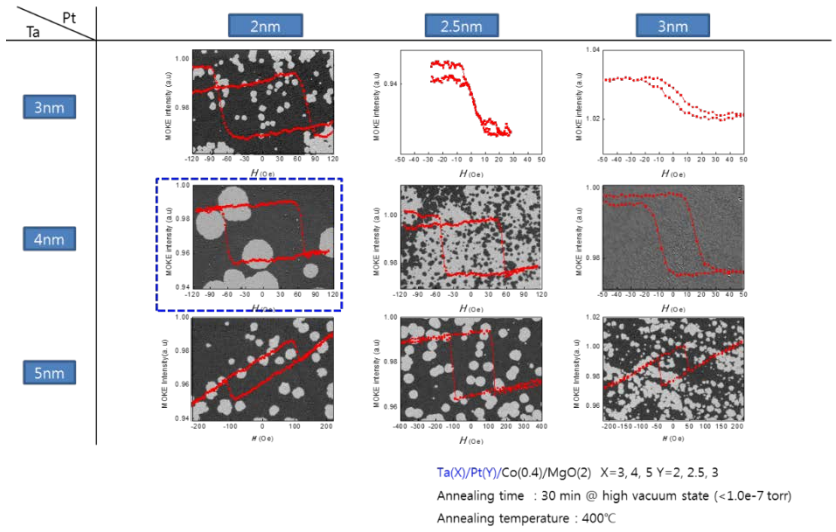

Figure 2.7. Optimization of Pt and Ta seed layer for large DW pattern. For large DW pattern, we choose a Ta 4 nm and Pt 2nm.

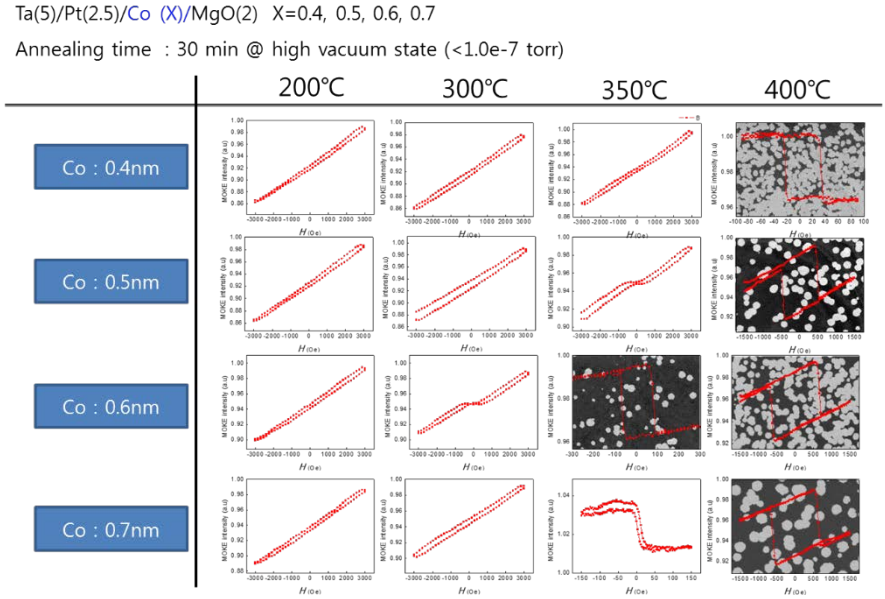

Figure 2.8 Annealing optimization of MgO PMA films. The annealing conditions above 350°C in high vacuum state are chosen for experiment which observed strong PMA with various Co thickness samples.

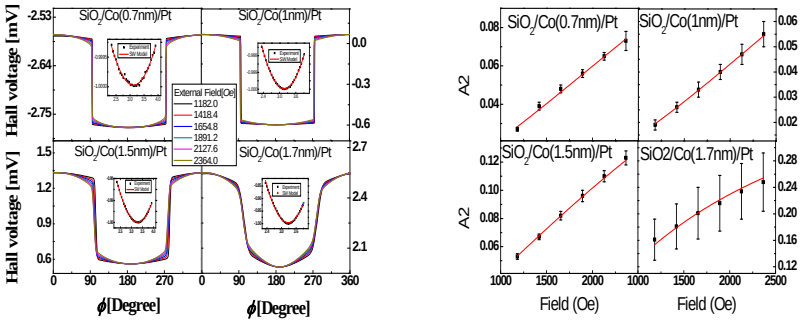

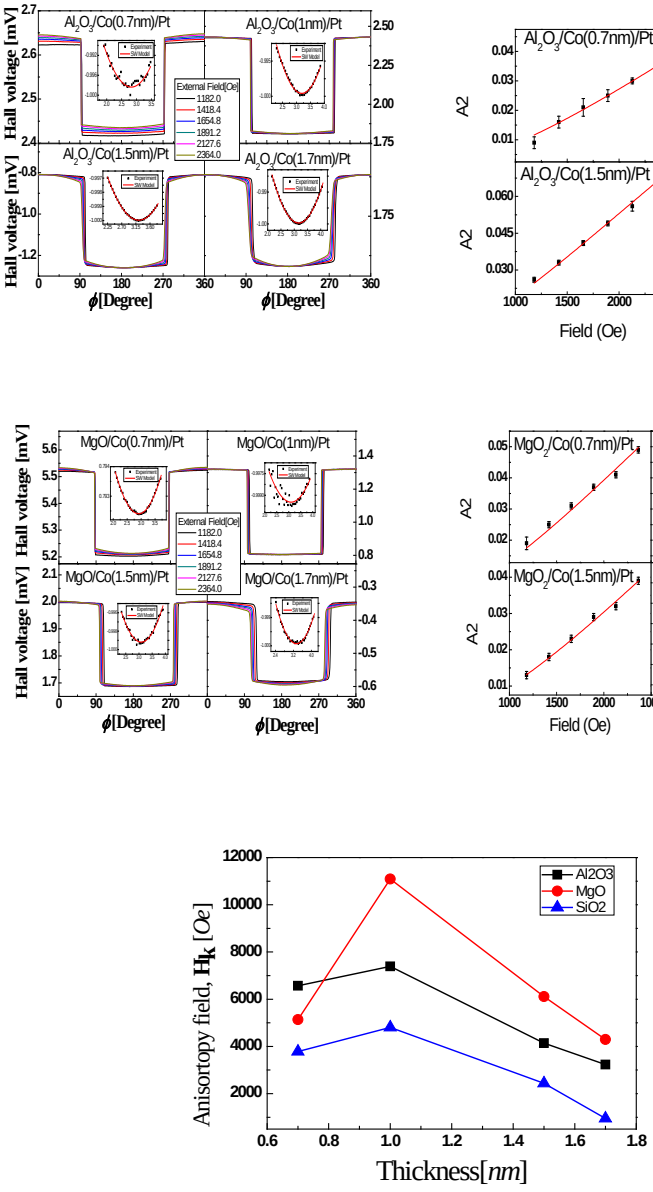

Figure 2.9 The anisotropy depend on Co thickness with various oxide(MgO, SiO_2, Al_2O_3) / Co(t) / Pt PMA films. The anisotropy field H_k is measured by extraordinary Hall effect torque method [25].

2.4 Sample fabrication for experiment of Gilbert damping experiment

2.4.1 CoFeB thin films

CoFeB film is one of the candidates for the next-generation nonvolatile random access memory because of its small Gilbert damping. The Gilbert damping constant α is related to the critical current density and the domain wall speed by the spin transfer torque. The CoFeB film has been therefore extensively examined for the potential application for the STT-MRAM and the domain wall device. For this study, we are optimized Gilbert damping constant with changing a material attached CoFeB layer, thickness of CoFeB, annealing temperature.

Previous report, the spin waves are generated by thin film structure which exchange interaction cannot be ignored due to its length/depth scale (nano-scale). It is therefore fundamentals for spin wave generation experiment with optimized Gilbert dapming constant. Figure 2.10 shown a various films structure of CoFeB thin films and its AMF image of surface state at as-deposite state. We reported an optimization process of Gilbert damping will be discussed in chapter 3.

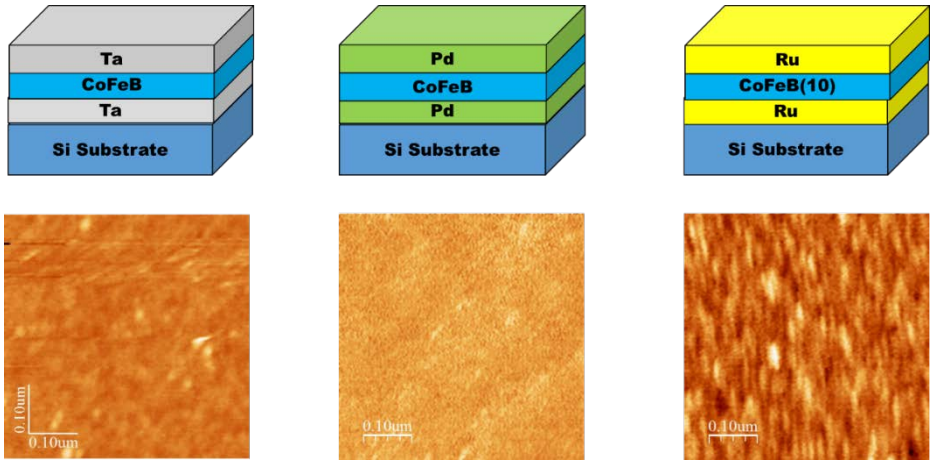

Figure 2.10. Various CoFeB thin films with its surface state with as-deposite state. The surface state observed using AFM.

2.5 Sample fabrication for experiment of Spin-orbit torque and Dzyaloshinskii-Moriya interaction

2.5.1 Pt/Co/X (X= 3d, 4d, 5d transition metal) structure

In recent study, DW motion has great improved by SOT and DMI due to its physical origin. The spin Hall effect and Rashba effect are develop as independent method, however, each result are same operation in SOT[26, 27]. The SOT explained by spin Hall effect is originated by spin current via non-ferromagnetic heavy metals. The SOT explained by Rashba effect is originated by interface between ferromagnetic layer and heavy metal. In this study, we investigate various metallic ferromagnetic film for enhancing a SOT using different spin Hall angle metals. This PMA films, in addition, have different interface of Co layers, which affect the Rashba effect.

We are firstly fabricate an optimized sample structure, which are Ta 5nm / Pt 2.5 nm / Co 0.6 nm / *X* 5nm films with various *X* by 3d, 4d, 5d metals. We choose a *X* by Ti(3d), Ru,(4d), Pd(4d), Ta(5d), W(5d), Au(5d) and Mg.(The Mg sample structure is Ta 5nm / Co 0.3nm/ Mg 5nm for large DW motrion, which pattern is changed to dendrite growth when increasing Co thickness.) Figure 2.11 shown film hysteresis loop with its DW pattern image. It has clear circular DW exist which available for SOT and DMI experiment. Experimental details will be discussed in chapter 4

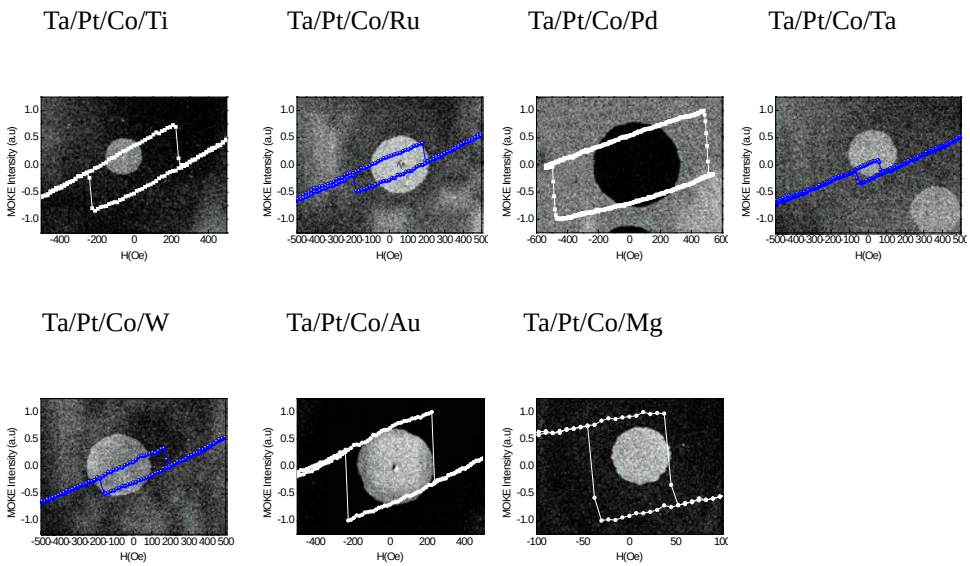

Figure 2.11 The various PMA films of Ta/Pt/Co/X structure. (X: Ti(3d), Ru,(4d), Pd(4d), Ta(5d), W(5d), Au(5d) and Mg)

2.5.2. Pt/Co/Mg/Pt structure

Recent study, there is remarkably development in the investigation of current induced DW motion for major candidate for next generation memory. Discovery of DMI in the Ultra-thin films with PMA and Mechanism of SOT are expected that spin torque memory have a high spin torque efficiency. It is, therefore, crucial problem to establish a chiral DW structure in the PMA films.

We firstly demonstrate DMI sign change using Mg layer insertion to Pt/Co/Pt PMA films. For finding a critical thickness of changing DMI, we are increasing a insertion thickness of Mg. Figure 2.12 shown a clear circular DW observed even inserting Mg layer. This sample check a DMI sign using asymmetric DW expansion method. It will , after then, check the SOT for finding a origin between SOT and DMI with its correlation. Chapter 5 will be discuss about this physical origins.

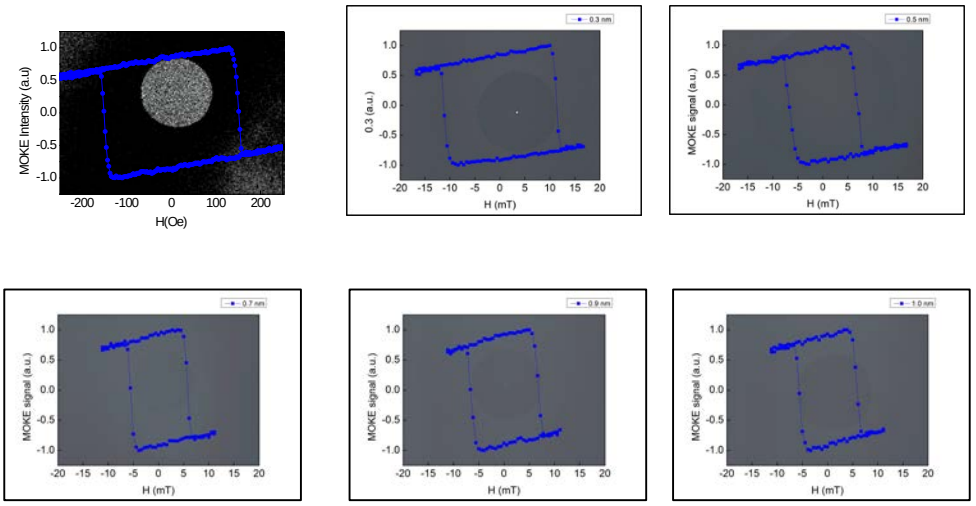

Figure 2.12 Pt/Co/Mg/Pt structure for demonstrating DMI sign change

Reference

[1] U. Gradmann and J. Müller, *Phys. Status Solidi* 27, 313 (1968)

[2] P. F. Carcia et al., *Appl. Phys. Lett.* 47, 178(1985).

[3] P. Bruno, *Phys. Rev. B* 39, 865 (1989); in Physical Origins and Theoretical Models of Magnetic Anisotropy (Ferienkurse des Forschungszentrums Jülich, Jülich,1993).

[4] B. Kaplan and G.A. Gehring “The domain structure in ultrathin magnetic films.” *J. Magn. Magn. Mater.* 128, 111(1993)

[5] M. Speckmann et al. *Phys. Rev. Lett*. 75, 2035(1995)

[6] N. Nakajima et al. *Phys. Rev. Lett*. 81, 5229 (1998)

[7] D. Weller et al, *Phys. Rev B* 49, 12889 (1994)

[8] G.H.O. Daalderop et al. *Phys. Rev. B* 50, 9989 (1994)

[9] H. R. Kaufman et al. *J. Vac. Sci. Technol. A* 3, 1774 (1985)

[10] S.-B. Choe. *Appl. Phys. Lett*. 92, 062506 (2008).

[11] S.-B. Choe and S.-C. Shin, *Appl. Phys. Lett.* 80, 1791 (2002)

[12] S.-B. Choe and S.-C. Shin, *J. Appl. Phys.* 87, 5076 (2000)

[13] S.-B. Choe and S.-C. Shin, *J. Appl. Phys*. 81, 5743 (1997)

[14] S.-B. Choe et al,. *Phys. Rev. B.* 70, 014412 (2004)

[15] K.-J. Kim et al.. *Nature* (London) 458, 740 (2009).

[16] Ruqian Wu et al., *J. Magn. Magn. Mater.*99, 71(1991)

[17] Mahdi Jamali et al, *Phys. Rev. Lett* 111, 246602 (2013).

[18] I. M. Miron et al, *Nature* 476, 189 (2011).

[19] S.-G. Je et al, *Phys. Rev. B* 88, 214401 (2014)

[20] A. Manchon et al., *J. Appl. Phys*. 104, 043914 (2008).

[21] J-.C. Lee et al., *IEEE Trans. Magn.* 46, 2009(2010)

[22] R. Shimabukuro et al., *Physica E* 42, 1014 (2010).

[23] H. X. Yang et al., *Phys. Rev. B* 84, 054401 (2011).

[24] B. Rodmacq et al., *Phys. Rev. B* 79, 024423 (2009)

[25] K.-W. Moon et al., *Rev. Sci. Instrum.,* 80, 113904 (2009); C-G. Cho M.S thesis. Seoul National University(2010)

[26] Mahdi Jamali et al., *Phys. Rev. Lett* 111, 246602 (2013).

[27] I. M. Miron et al, *Nature* 476, 189 (2011).

Chapter 3

Gilbert damping

CoFeB films have been extensively examined as one of the candidates for the next-generation nonvolatile random access memory [1] and domain wall devices [2]. In the current-driven domain-wall motion, the Gilbert damping constant is known to be related to the critical current density and the domain wall speed. To adjust the Gilbert damping constant, it is common to adopt several method. 1) We are observing a CoFeB thickness dependence of Gilbert damping. 2) We choose a proper seed/capping layer for optimizing Gilbert damping by reducing a spin pumping. 3) We finally report an experimental observation of the annealing temperature dependence of Gilbert damping.

Gilbert damping constant is measured by time-resolved MOKE(TR-MOKE) and ferromagnetic resonance technique. The change of the magnetic and structural properties is examined by use of a vibrating sample magnetometer (VSM) as well as an x-ray diffractometry (XRD). The results show that optimized Gilbert damping are severely dependent on the materials of the capping/under layers, thickness and annealing temperature. The correlation with the magnetic and structural properties will be discussedThis chapter reviews magnetic field driven DW dynamics including dimensionality problems. The purpose of this chapter is to investigate the physical mechanism of magnetic field driven DW dynamics for the case of DW propagation along the nanowire or DW depinning from a constriction in thermally activated regime.

3.1 Introduction

The CoFeB amorphous thin film is the most promising candidate in Spin-transfer-torque magnetic tunnel junction(STT-MTJ) and Spin-transfer-torque domain wall(STT-DW) device. It is reported that the CoFeB thin film have a small Gilbert damping constant, which reduces the critical current density Jc of STT-MTJs[3] and enhances the velocity of domain wall of STT DW devices [2].

In this section, the Gilbert damping constant is introduced as major parameter of spin torque device. The memory applications of Gilbert damping are shown that understanding a physical origin is important with fabricating a device.

From chapter 1, we are starting from Landau-Liftshitz-Gilbert(LLG) equation. The magnetic wire with 1 dimensional freedom, which DW describes as its position and angle, can be expressed as follow equation [4],

$$\begin{aligned}\left(1+\alpha^2\right)\dot{q} &= -\frac{\alpha\gamma\Delta}{2M_S}\left(\frac{\partial\varepsilon}{\partial q}\right)+\frac{\gamma\Delta}{2}H_K\sin\left(2\psi\right)+\left(1+\alpha\beta\right)u \\ \left(1+\alpha^2\right)\dot{\psi} &= -\frac{\gamma}{2M_S}\left(\frac{\partial\varepsilon}{\partial q}\right)-\frac{\gamma\alpha}{2}H_K\sin\left(2\psi\right)+\left(\beta-\alpha\right)\frac{u}{\Delta}\end{aligned} \tag{3.1}$$

In the current driven DW motion situation with no pinning assumption and with large β, this equation modified as follow equation [5],

$$\begin{aligned}\left(1+\alpha^2\right)\dot{q} &= +\frac{\gamma\Delta}{2}H_K\sin\left(2\psi\right)+\left(1+\alpha\beta\right)u \\ -\frac{\Delta}{\alpha}\left(1+\alpha^2\right)\dot{\psi} &= +\frac{\gamma\Delta}{2}H_K\sin\left(2\psi\right)+\left(1-\frac{\beta}{\alpha}\right)u\end{aligned} \tag{3.2}$$

This equation implies the velocity of DW $v = \dot{q} \propto \frac{\beta}{\alpha}u$ with Gilbert damping constant α. It is therefore an optimal strategy with decreasing Gilbert damping constant for high performance DW device. The applications of Gilbert damping are STT-MRAM and spin wave logic device. In STT-MRAM, there is major parameter to engineering which called switching current. Each cell of STT-MRAM have an intrinsic switching current that this critical current is related on material. Previous reports [3], the switching current is described as $I_{Switing} = \alpha\frac{\gamma e}{\mu_B g}M_s H_K V = 2\,\alpha\frac{\gamma e}{\mu_B g}E$. This means that small Gilbert damping constant make easy to switching a magnetization in STT-MRAM. In spin wave logic device, the major parameter to engineering is life time of spin wave. The life time is also related on Gilbert damping constant. Previous reports[6, 7], the life time of spin wave is described as $\tau = \frac{1}{\omega\alpha}$. This means that small Gilbert damping constant make long life time of spin wave. From this motivation, we are fabricated optimal structure for small Gilbert damping constant.

3.2 Measurement technique

3.2.1 Ferromagnetic Resonance technique

The conventional way to measure a Gilbert damping constant α is ferromagnetic resonance (FMR) technique. This technique is based on cavity resonator which stores the microwave energy. The resonance frequency f_0 of this cavity resonator have no reflect microwave that means maximizing a magnetic field without electric field by geometric property of resonator. We use a rectangular cavity which designed the f_0 is 9.5GHz in th TE_{102} mode [8]. This homemade rectangular cavity resonator is well performed the magnetic field (H) dependence FMR experiment by using above few nm ferromagnetic thin films. Figure 3.1 shown a schematic of cavity FMR. From the absorption spectra, we derivative the line spectra that obtained a first derivation of absorption provide the α by using ΔH_{pp}. The ΔH_{pp} is as follow [9,10].

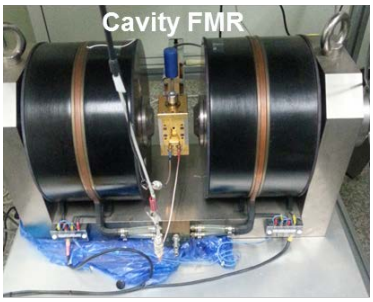

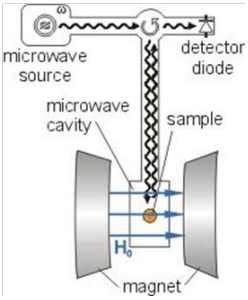

Figure 3.1 Schematics of Cavity-FMR. This cavity was designed for reducing an eddy current effect[8]

$$\Delta H = \frac{\alpha}{\left|\frac{d(2\pi f_0)}{dH}\right|}\frac{\gamma}{M_s}\left(\frac{\partial^2 E}{\partial {\theta_M}^2} + \frac{1}{sin^2\theta_M}\frac{\partial^2 E}{\partial {\varphi_M}^2}\right) \tag{3.3}$$

Where E is the magnetic free energy, Ms is saturation of magnetization, γ is gyromagnetic ratio, θ_M and φ_M are the polar and the azimuthal equilibrium angles of magnetization vector. If M is fully saturated, the equation 3.3 derived as

$$\alpha = \frac{\sqrt{3}\gamma\Delta H}{4\pi f_0} \tag{3.4}$$

From this relation, we are analyze a first derivation spectra to determine a Gilbert damping constant.

3.2.2 Time-resolved magneto-optical Kerr effect

For high resolution technique for observation a Gilbert damping, we are using a time-resolved MOKE (TR-MOKE) system. This system developed by optical pump-probe method with femtosecond laser. Figure 3.2 shown a schematic of TR-MOKE. The magnetization of the film is excited by optical pulse. This pulse beam called the pump beam. After excitation, the magnetization interrogated by the probe beam at a delay time τ. Time resolution could be obtained by this stroboscopic process. For this study, we use a 100 fs Ti:sapphire laser pulse with 94MHz repetition rate and 800 nm wavelength as a pump beam. We are then second-harmonic laser pulse of 400 nm wavelength were used as probe beam. The pump beam is focused onto a spot with a diameter ~ 1 μm and magnetic field of 2.5kOe is applied at an angle 10° from the sample normal. The Gilbert damping constant was determined based on the LLG equation for precession analysis. Using polar coordinated and external field H_{app}, LLG equation can be derived as,

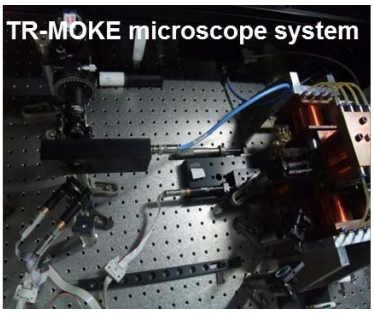

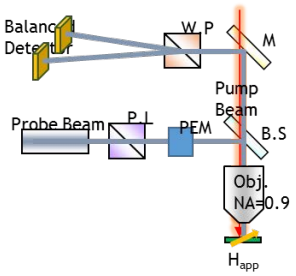

Figure 3.2 Schematics of TR-MOKE. This system have focused spot ~1 μm

$$\dot{\theta} = \frac{\alpha\gamma}{1+\alpha^2}\left(H_{app,y}\cos\theta\sin\varphi - H_{app,z}\sin\theta + M_s\cos\theta\sin\theta\right) + \frac{\gamma}{1+\alpha^2}H_{app,y}\cos\varphi$$

$$\sin\theta\dot{\varphi} = -\frac{\gamma}{1+\alpha^2}\left(H_{app,y}\cos\theta\sin\varphi - H_{app,z}\sin\theta + M_s\cos\theta\sin\theta\right) + \frac{\alpha\gamma}{1+\alpha^2}H_{app,y}\cos\varphi \quad (3.5)$$

This measurement system, in addition, have a position scanned by tilting half mirror in the setup. Previous report, the ultrafast demagnetization is possible source of the propagation of spin waves which could be detected by TR-MOKE [12]. We are also observation of spin wave propagation in this sample, which is possible applicant for spin wave generation.

3.3 Optimization of Gilbert damping constant

3.3.1 Thickness dependence of Gilbert damping

We are fist demonstrate a thickness dependence of Gilbert damping constant. The seed/capping layer are fixed as Ta layer with 1nm thickness. The CoFeB layer as a ferromagnetic layer has been chosen for small Gilbert damping constant [1]. The Gilbert damping constant will be decreased as thickness of CoFeB increased. This is because the physical origin of Gilbert damping from its energy dissipation channel. The increasing volume of CoFeB layer is make an energy dissipation channel relatively small. This mechanism with spin pumping by exchange magnon is intensively studied by recent researchers [13, 14]. From this reports, the energy dissipation channel by spin waves are generated above critical thickness of CoFeB layer. This means the dissipation channels are came into interface between ferromagnetic layer and non-magnetic layer. In our experiment, It is clearly shown the tendency depend on thickness increase [Figure 3.3].

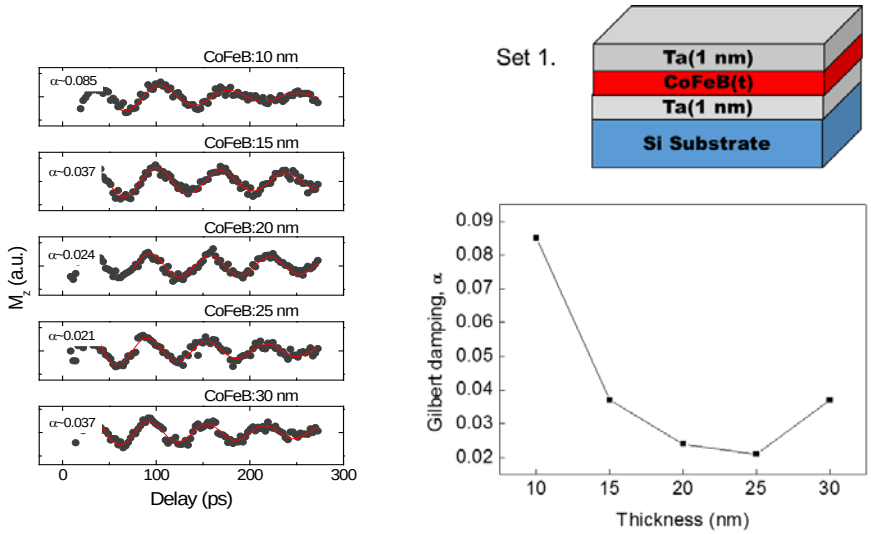

Figure 3.3 The CoFeB thickness dependence of Gilbert damping constant.

The minimum Gilbert damping constant observed in 25 nm thickness of CoFeB which is fixed for next optimization step. The 30nm thickness of CoFeB samples which enhanced Gilbert damping constant are used for spin wave experiment.

3.3.2 Seed/Capping layer effect of Gilbert damping

The appropriate adjacent layer had been intensively studied in Gilbert damping related research. Due to its spin pumping, adjacent layer enhance a Gilbert damping constant [13]. In this section, adjacent layer are investigated for optimized Gilbert damping constant. We choose a material by sandwich

structure with Ta, Ru, Pd. The total structure, therefore, are X 5nm / CoFeB 10 nm / X 5nm on the Si substrate with natural oxide by X are Ta, Ru, and Pd. Figure 3.4 shown a first derivatives of FMR absorption spectra. This indicated that Ta has smallest spin pumping and Pd has largest spin pumping.

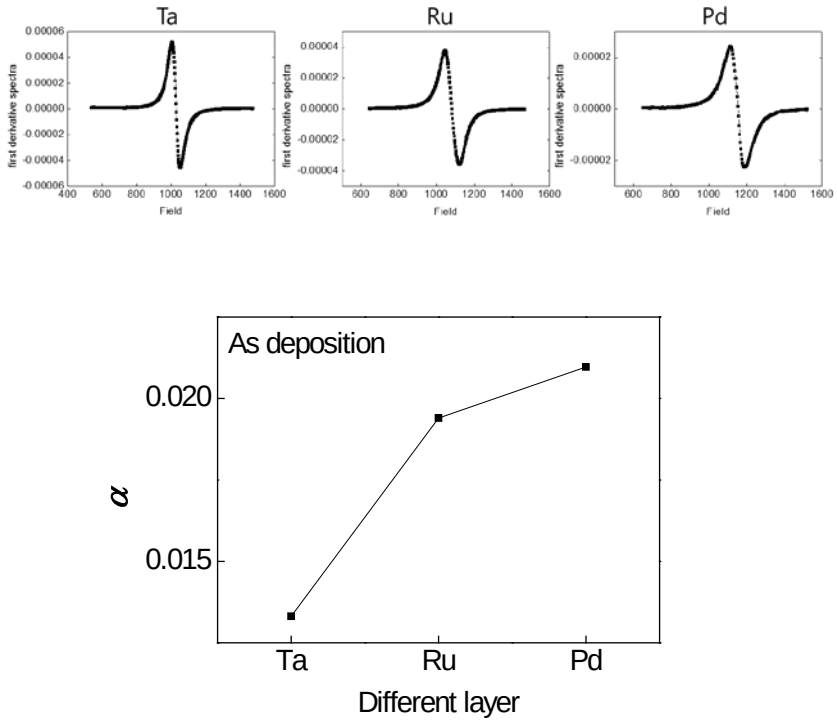

Figure 3.4 The first derivatives of FMR absorption spectra of Ta, Ru, Pd samples

3.3.3 Annealing effect on Gilbert damping

Recent experiments on the CoFeB thin films have shown that the Gilbert damping constant can be manipulated by either choosing the

appropriate materials for the adjacent nonmagnetic layers [15] or adjusting the proper annealing process [16]. Since the magnetic properties of the films are very sensitive to the atomic mixing between the CoFeB and adjacent layers [17] during the annealing process, it is essential to optimize the appropriate annealing procedure depending on the properties of the adjacent nonmagnetic layers. Here, we investigate the effect of the annealing temperature on the Gilbert damping constant and the coercive field of the CoFeB films with several different adjacent layer materials. To find the origin of the effect, the surface roughness of the samples is examined and then, compared with the variation of the Gilbert damping constant and the coercive field.

The amorphous CoFeB thin films are annealed in high vacuum ($<5x10^{-8}$ torr) for 2 hours without any magnetic field. The annealing temperature T_A is varied from 200°C to 400°C with 100°C steps.

Figure 3.5 illustrates the typical c-FMR measurement results on the derivative spectra with respect to the external magnetic field H. The figure clear shows the typical absorption spectra with two derivative peaks. The peak-to-peak linewidth ΔH_{pp} quantifies α by use of the relation $\alpha=\sqrt{3}\gamma\Delta H_{pp}/2\omega_0$ [18], where γ is the gyromagnetic ratio. The measured values of α are plotted with respect to T_A for Ta-, Ru-, and Pd-Samples in Figure. 3.5.

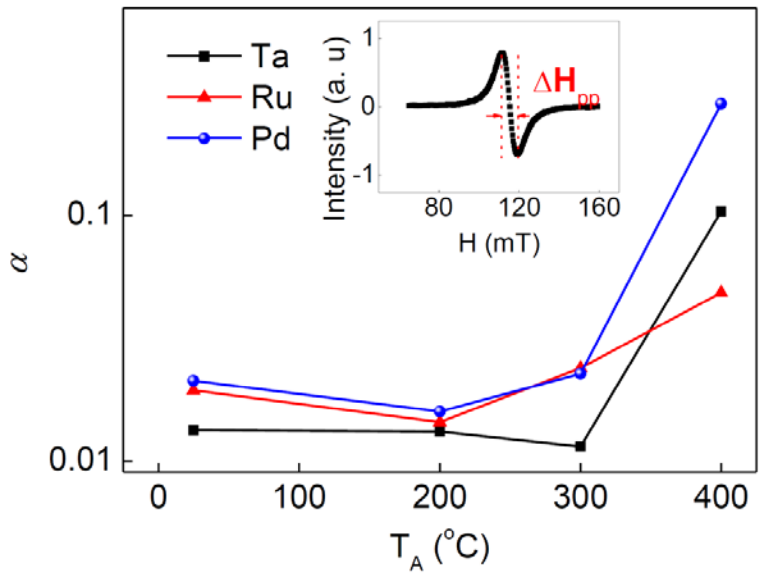

Figure 3.5 The typical c-FMR measurement results on the derivative spectra with respect to annealing temperature.

As T_A increases, α is slightly decreased first and then, increased again as seen in Figure. 3. 5. Thus, the minimum value of α is attained at T_A=300°C for Ta-Sample and at T_A=200°C for Ru- and Pd-Samples, respectively. The decrement of α at the small T_A regime is well understood since the annealing enhances the crystalline structure of the sample by removing the defects and imperfections in the as-deposited states. It has been reported that the diffusion of the B atoms is dominated in the annealing process of the CoFeB layers [19,20] and thus, the CoFe crystallization might be the major origin of the α reduction.

On the other hand, the increment of α at the higher T_A regime is possibly caused by severe atomic intermixing between the magnetic and

adjacent nonmagnetic layers and/or development of the polycrystalline grains[19,13]. To examine the grain formation with respect to T_A, the surface images of the samples are obtained by use of an atomic force microscope (AFM). Figure 3.6 shows the surface images of 200°C- and 400°C-annealed samples with different adjacent layer composition. The figure clearly shows that all the 400°C-annealed samples exhibit rougher surface and larger grains, compared to the 200°C-annealed samples. Such grain formation thus limits the range of T_A in the annealing process, $T_A \leq 300$°C for Ta-Sample and at $T_A \leq 200$°C for Ru- and Pd-Samples, respectively

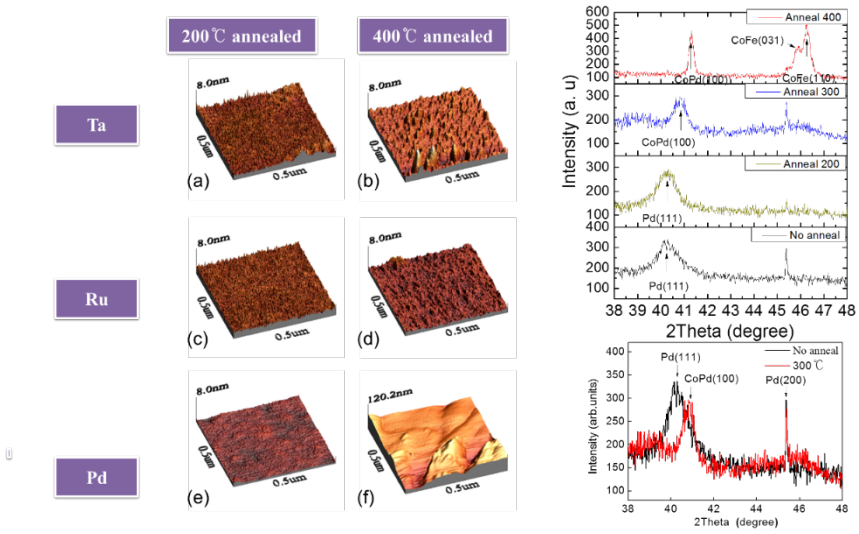

Figure 3.6 The structural analysis of CoFeB film with respect to annealing temaperature. AFM and XRD data shown an interface roughness changing and atomic mixing.

3.3.4 Correlation between Gilbert damping and structural modification

To examine the grain formation with respect to T_A, the surface images of the samples are obtained by use of an atomic force microscope (AFM). Figure 3.7 shows the surface images of 200°C- and 400°C-annealed samples with different adjacent layer composition. The figure clearly shows that all the 400°C-annealed samples exhibit rougher surface and larger grains, compared to the 200°C-annealed samples. Such grain formation thus limits the range of T_A in the annealing process, $T_A \leq 300$°C for Ta-Sample and at $T_A \leq 200$°C for Ru- and Pd-Samples, respectively.

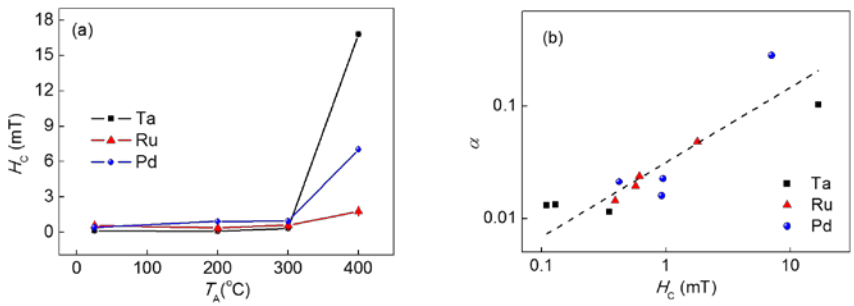

Figure 3.7. The empirical relation between H_c and Gilbert damping constant. . (a) H_C with respect to T_A for Ta-, Ru-, and Pd-Samples. (b) Plot of α with respect to H_C.

The effects caused by the grain formation and the atomic intermixing

are again observed in the coercive field H_C variation with respect to T_A. Figure 3. 6. (a) shows H_C with respect to T_A for different adjacent layer materials. It is interesting to see that H_C shows a behavior similar to α: H_C is slightly decreased first and then, abruptly increased as T_A increases. It is therefore worthwhile to examine the correlation between H_C and α. Figure 3. 6.(b) shows the plot of α vs H_C. The figure clearly shows the existence of the correlation between H_C and α, which can be best described by an empirical equation $\alpha=(H_C/H_0)^{\zeta}$ with $H_0=6.833\times10^{-4}$ mT and $\zeta=2/3$. The present empirical relation enables one to optimize the sample properties routinely by the coercive field measurement, before carrying out the relatively-sophisticated damping constant measurement

Reference

[1] S. Mangin, D. et al,. *Nat. Mater.* 5, 210 (2006)

[2] S. Fukami, et al., *Appl. Phys. Lett.* 98, 092504 (2011)

[3] S. Ikeda, et al., *Nature Mat*. 9, 721(2010)

[4] Luc Thomas, et al., *Nature* 443, 197 (2006)

[5] S.W Jung et al., *Appl. Phys. Lett*. 92, 202508(2008)

[6] C. Cheng et al. *Appl. Phys. Lett.* 103, 232406(2013)

[7] A. Khitun, et al., *IEEE.Trans.Mag* 44, 2141 (2008)

[8] L. Andreozzi, et al., . Optoelectron. 4, 55 (2005)

[9] D.L. Mills, S.M. Rezende. *Spin Dynamics in Confined Magnetic Structures*

II,

vol. 87, pp. 27~59, Springer, 2003,.

[10] K. Kobayashi, et al., IEEE Trans. Magn. 45, 2541 (2009)

[11] S.-I. Kim et al., *Curr. Appl. Phys*. 13, 1021 (2013)

[12] Y. Au, et al., *Phys. Rev. Lett*. 110, 097201 (2013)

[13] Y. Tsekovnyak and A. Brataas *Phys. Rev. Lett.* 88, 117601 (2002)

[14] C.W. Sandweg et al., *Phys. Rev. Lett* 106, 216601(2011)

[15] H. Lee et al., *J. Phys. D: Appl. Phys*. 41, 215001 (2008).

[16] Shaohai Chen et al., *Appl.Phys.Lett*. 103, 032402 (2013).

[17] Yanyan Zhu et al., *J. Appl. Phys*. 111, 07C106 (2012).

[18] B. Hinrich, J. F. Cochran, and R. hasegawa, J. Appl. Phys. 57, 3690 (1985).

[19] Jeon, B.-G. et al., *Jor. Kor. Mag. Soc.* 21, (6), 214 (2011).

[20] H. Bouchikhaoui, et al., *Appl. Phys. Lett*. 103, 142412 (2013).

[21] P. V Pauluskar, et al., *J. Appl. Phys*. 99, 08E503 (2006)

Chapter 4

Spin-orbit torque & Dzyaloshinskii-Moriya interaction

The spin-orbit torque (SOT) is are investigated with discovery of current induced domain wall motion along a current direction. The DW is governed by spin current due to its spin angular momentum transfer, which is propagated along a electron flow direction.[1,2] In Pt/Co/Pt PMA structure, there is, however, an opposite direction of DW motion which is first observation of DW motion only current flow [3]. From this reports, there is many experimental proof for DW propagation for current direction including a heavy metal / ferromagnetic layer / oxide structure [4]. This phenomena is called a SOT, which is related spin orbit coupling of adjacent metal layer and interface.

The Dzyaloshinskii-Moriya interaction (DMI) is also arise from the spin-orbit coupling between neighboring ions. In our experiment, this is also radical physics for current driven DW motion. The DMI field make a DW configuration to Neel wall structure. It is the internal field for determining a DW configuration which enhance the efficiency of SOT.

In this chapter, we are investigate SOT and DMI in Co films sandwiched by various 3d, 4d, and 5d transition metals. The sign and magnitude of the DMI and SOT are measured with asymmetric DW expansion and ω-2ω measurement method, respectively. The overall trend depending on the materials combination will be discussed

4.1 Introduction

4.1.1 Spin-orbit torque: Spin Hall picture vs. Rashba picture

Introduction

From discovery of SOT, there have been a controversy for current induced DW motion along the current direction. In the recent reports[4, 13], the Rashba effect and spin Hall effect are noticed as physical origin of SOT which are same effective torque on DW in current induced DW motion.

In spin Hall mechanism, the heavy metal (adjacent layer of Co layer) is source of incident spin current, which generate torque on Co magnetization. The incident spin current diffused from the heavy metal have a specific angular momentum which is possible to propagate a DW along the specific direction depend on its spin Hall angle sign/magnitude. This suggest a modified LLG equation as follows [14],

$$\frac{\partial m}{\partial t} = -\gamma m \times H_{eff} - \theta_{SH} c_J m \times \left(m \times \hat{y}\right) + \alpha m \times \frac{\partial m}{\partial t} - b_J m \times \left(m \times \frac{\partial m}{\partial t} \right) - \beta b_J m \times \frac{\partial m}{\partial x} \tag{4.1}$$

Equation 4.1 illustrate term of effective torque which is parallel to current direction and/or perpendicular to current direction. The Slonczewski-like SOT

(SL-SOT) term is current perpendicular direction as being like external field to sample in-plane direction. From the sign/magnitude of spin Hall angle, θ_{SH}, SL-SOT term determine a DW motion direction due to current injection. The measuring a spin current incident from a heavy metal layer is radical to analyze a SL-SOT. From the D. C. Ralph and R. A. Buhrman describe a spin current due to its strong spin-orbit coupling of heavy metal layer are more than 100 times larger than previous reports as use with Tantalum [13]. The other physical origin, the Rashba effect, due to its structure inversion asymmetry have the effective torque just same as spin Hall mechanism. The Rashba picture, the interfacial effect of symmetry broken structure, also modifying a LLG equation as follow [15].

$$\frac{\partial m}{\partial t} = -\gamma m \times H_{eff} - \gamma m \times H_R + \gamma\beta m \times \left(m \times H_R\right) + \alpha m \times \frac{\partial m}{\partial t} - b_J m \times \left(m \times \frac{\partial m}{\partial t} \right) - \beta b_J m \times \frac{\partial m}{\partial x} \tag{4.2}$$

Where H_R is $H_R = \frac{\alpha_R m_e P}{\hbar e M_s^2 (1+\beta^2)} \left(\hat{z} \times j_e\right)$. Equation 4.2 show the field-like SOT (FL-SOT) term is current parallel direction as being like external field to sample normal. The Slonczewski-like SOT (SL-SOT) term is current perpendicular direction as being like external field to sample in-plane direction. In this picture, SL-SOT term is totally same effect by interpretation of spin Hall picture. It is, therefore, hard to separate a physical origin in experimental

situation by using any current induced DW motion.

In this chapter, we choose transition metal for enhancement of SOT with spin Hall picture. The transition metal of 3d, 4d and 5d have a various spin Hall sign/magnitude due to its spin orbit coupling. The seed/capping layer of Co ultra-thin film have great effective field-like torque using combination of 3d, 4d, 5d transition metal as illustrated follow figure 4.1. The strategy is simple way to increase an effective spin current due to its different sign/magnitude of spin Hall angle of seed/capping layer. The dependence of material selection will be discussed in section 4.3.

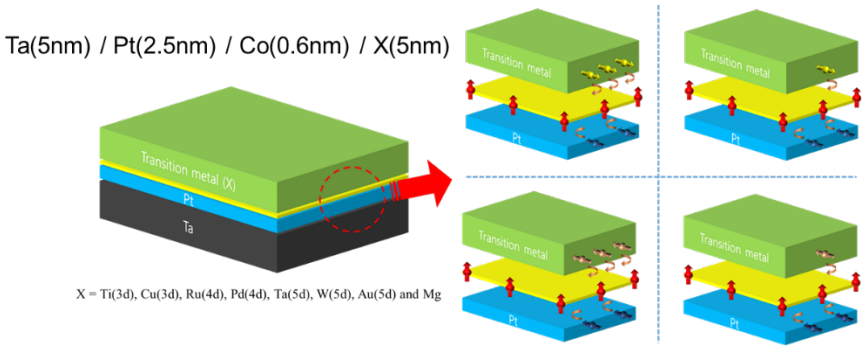

Figure 4.1 The Co films with PMA sandwiched by various 3d, 4d, 5d transition metals

4.1.2 Dzyaloshinskii-Moriya interaction

From the discovery of Dzyaloshinskii-Moriya interaction (DMI), there is a new challenge of engineering a DW configuration for high efficiency

spin torque device. The DMI also have a physical origin related on spin orbit coupling. In atomic aspect, the spin-flip with two atoms are both same energy state, which is called Heisenberg exchange interaction. It has, however, difference energy state when spin-flip with two atoms along the third atom involved. Figure 4.2 illustrate the both of spin-flip state. In a second order perturbation theory, this antisymmetric exchange term is derived as $D_{ij}\cdot(\boldsymbol{S}_i\times\boldsymbol{S}_j)$ [16]. $\boldsymbol{S}$ is denoted the spin of each atoms and $\mathbf{D}_{ij}$ is Dzyaloshinskii vector which derived by the scattering calculus with considering a spin-orbit coupling [17]. The DW with DMI, the antisymmetric exchange term, have a modification to type of DW with chiral structure known as effective direction of DW propagation. In general case without DMI, the Néel wall is more unstable than Bloch wall because of its magnetostatic energy [18].

For considering DMI, $\boldsymbol{S}_i$ is $\mathbf{m}$(x) and $\boldsymbol{S}_j$ is $\mathbf{m}$(x) + $\frac{\partial \boldsymbol{m}}{\partial x}$, which stand for a $-\nabla_{\hat{m}}$ of DW energy. The DMI field originated from this energy equation known as an induced internal field only in x axis [19]. For this physical situation, we establish a chiral DW(Néel wall) structure by using combination of a seed/capping layer with different spin-orbit coupling. These sample set also enhance the efficiency of SOT. It is, furthermore, an origin which specific chirality of DW could move DW along a current direction due to incident current. In section 4.3, we discuss about combination of material with qualitative/quantitative analysis. In section 4.5, we suggest a method of controlling DMI using result of section 4.3.

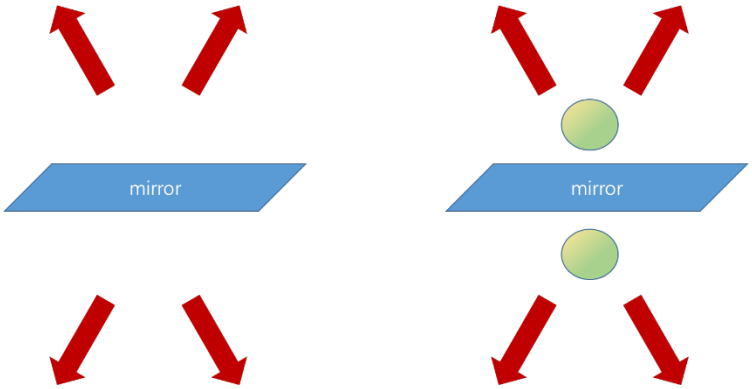

Figure 4.2 Illustration of spin-flip state. The left has no energy difference. The right, however, has energy difference within structure inversion asymmetry

4.2 Measurement technique and analysis

4.2.1 Measurement technique of spin-orbit torque

For measuring a SOT, the recent reports proposed a ω-2ω measurement method using tilting of the spin orientation [8, 9, 20~22]. The current induced DW motion is illustrated by the effective field on the magnetization in the experimental situation. The extraordinary Hall voltage is monitored as function of external field and current induced torques. The tilted magnetization by in-plane field could be oscillated when the ac current are applied in that system. The Hall voltage dependence of current could be expanded as first order approximation. There is, however, an electrical artifact in this method due to its in-plane component of magnetization as called planar

Hall effect(PHE). To get rid of PHE on harmonic voltage, PHE are observed on φ direction 0 to 360 degree. This measurement is one of conventional method for determine a SOT, which is used in our experiment.

For the accurate SOT measurement, another measurement method is developed in last few years. The ferromagnetic resonance technique is developed for measuring a SOT in heavy metal / ferromagnetic layer / oxide heterostructure [13]. This measurement report a spin Hall angle due to its spin orbit coupling of heavy metal layer. The measurement method is called as spin torque ferromagnetic resonance (ST-FMR) [23]. This method determine a spin Hall angle without dependence of anisotropic magnetoresistance(AMR) corresponding to signal arise from field symmetric/antisymmetric part of the dc voltage. It is, however, the spin diffusion length of adjacent layer and its inverse spin Hall effect make a discrepancy of spin Hall conductivity and spin Hall angle, which data from ST-FMR should be carefully analyzed.

The other method of measuring a SOT is optical measurement using MOKE microscopy. The PHE does not appear in optical measurement, which have reduced other artifact (Anomalous Nernst effect, AMR, PHE, etc.) for exact SOT analysis. This method is also based on ω-2ω measurement method with harmonic voltage analysis. The magnetization signal due to moderate ac current is monitored by MOKE signal. The SOT of Pt/Co/Mg/Pt structure is observed by this optical measurement method. The dependence of Mg insertion will be discussed in chapter 5.

4.2.2 Analysis data of spin orbit torque experiment

Figure 4.3 illustrate a schematics of experimental set-up and coordinate systems. The positive current is defined as current along the +X direction from Ti/Au pad. The extraordinary Hall voltage are used to observing SOT in Pt/Co/X sample set. Figure 4.4 show the material (X: Ti(3d), Ru(4d), Pd(4d), Ta(5d), W(5d), Au(5d), and Mg) dependence of ω-2ω signal by using electrical measurement. From the small oscillation due to the ac current, the Hall voltage is describe as follow [8],

$$\begin{aligned} V &= IR = I_0 \sin\omega t \cdot R\left(\vec{H} + \Delta\vec{H}\sin\omega t\right) \\ &= I_0 \sin\omega t \cdot \left[R\left(\vec{H}\right) + {dR}/{d\vec{H}} \circ \Delta\vec{H}\sin\omega t \right] \end{aligned} \tag{4.3}$$

We consider the resistance from both of extraordinary and planar Hall effect as follow

$$R = R_{EHE}\cos\theta + R_{PHE}\sin^2\theta\sin\varphi\cos\varphi \tag{4.4}$$

The anisotropy field is measured by extraordinary Hall torque [25] with external in-plane field $\boldsymbol{H}_x$, which determine θ information. For a small θ, R_ω and $R_{2\omega}$ is derived as equation 4.5.

$$R_\omega = R_{EHE}\cos\theta_0 + R_{PHE}\sin^2\theta_0\sin\varphi_0\cos\varphi_0$$

$$R_{2\omega} = -\frac{1}{2}\left[R_{EHE}\frac{d\cos\theta}{d\vec{H}}\bigg|_{\theta_0} \circ \Delta\vec{H} + R_{PHE}\frac{d\left(\sin^2\theta\sin\varphi\cos\varphi\right)}{d\vec{H}}\bigg|_{\theta_0} \circ \Delta\vec{H} \right]$$

(4.5)

The θ and φ component of effective field are thus derived as,

$$H_\theta\left[\left(R_{AHE} - R_{PHE}\cos\theta_0\sin 2\varphi_0\right)\frac{d\cos\theta}{dH_\theta}\bigg|_{\theta_0} \right] + H_\varphi\left[R_{PHE}\sin^2\theta_0\cos 2\varphi_0\frac{d\varphi}{dH_\varphi}\bigg|_{\varphi_0} \right]$$

(4.6)

In this analysis of SOT, it give a conflicting result if the PHE is not relatively smaller than EHE and local $\boldsymbol{H}_{\mathrm{k}}$ distribution exist due to its current density. For the precise analysis of SOT, we adapt the optical measurement by using MOKE microscopy. In this case, the measurement signal is analyzed based on LLG equation with presence of SOT.

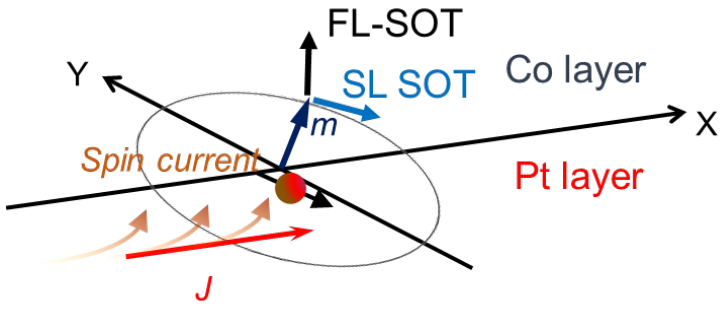

Figure 4.3 Schematics of experimental set-up and coordinate systems using spin Hall picture

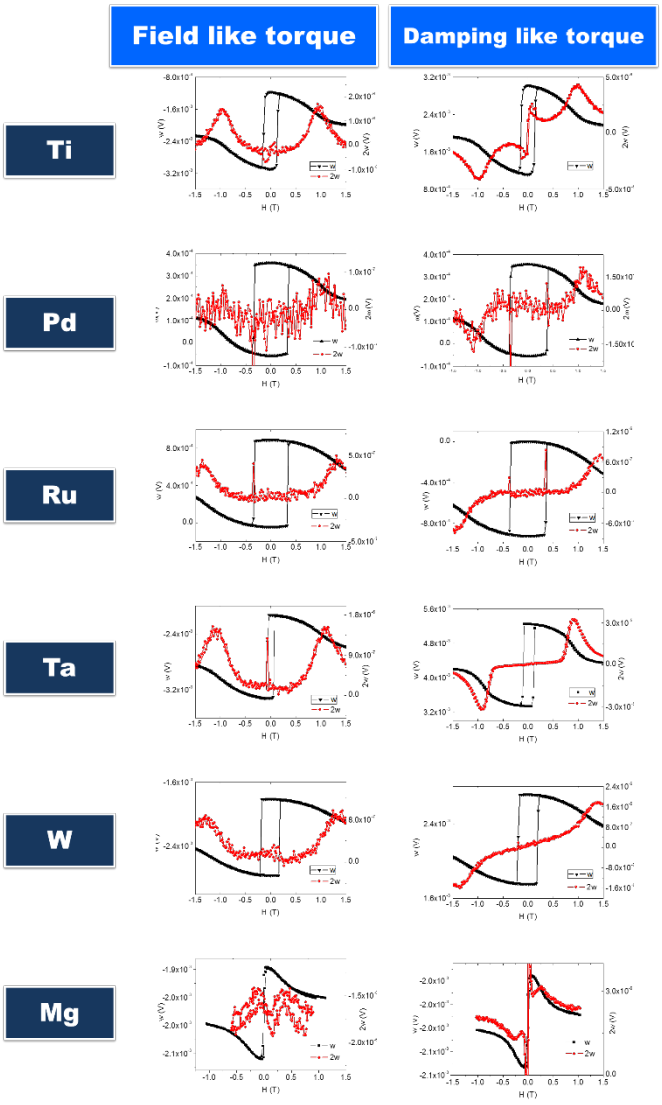

Figure 4.4 The Pt/Co/X structure (X: Ti(3d), Ru(4d), Pd(4d), Ta(5d), W(5d) and Mg) X dependence of ω-2ω signal by using electrical measurement are shown.

The equation 4.7 shows a LLG equation with presence of SOT which considered a longitudinal and transverse torque [26].

$$\frac{\partial \hat{m}}{\partial t} = -\gamma \hat{m} \times \left(\vec{H}_{ext} + \vec{H}_{ani}\right) + \alpha \hat{m} \times \frac{\partial \hat{m}}{\partial t} - \gamma H_T(\hat{m} \times \hat{y}) + \gamma H_L(\hat{m} \times (\hat{m} \times \hat{y})$$

(4.7)

Where $\boldsymbol{H}_{\text{ani}}$ is an anisotropy field, $\boldsymbol{H}_{\text{ext}}$ is external field, $\hat{m}$ is Magnetization unit vector, γ is gyromagnetic ratio, and $H_{L,T}$ are effective longitudinal/transverse magnetic field, respectively. More detail calculation will be introduced in Appendix I. From the equilibrium state, the cos θ is

$$\cos\theta = 1 - \frac{(H_x + H_L)^2 + \left(H_y + H_T\right)^2}{2(H_z + H_k)^2}$$

(4.8)

When the ac current was applied with its frequency ω, the effective field $H_{L,(T)}$ is derived as $H_{L,(T)} = J_0\beta_{L,(T)} \sin \omega t$. The J_0 is current density, and $\beta_{L,(T)}$ is efficiency of SOT. The cos θ is could be derived as

$$\cos\theta = 1 - \frac{(H_x + H_L)^2}{2(H_z + H_k)^2} - \frac{J_0\left(\beta_L H_x + \beta_T H_y\right)}{(H_z + H_k)^2} sin\omega t - \frac{{J_0}^2\left(\beta_L + \beta_T\right)^2}{2(H_z + H_k)^2} sin^2\omega t$$

(4.9)

From this relation, we determine an effective field of longitudinal/transverse

SOT. Figure 4. 5 shows a result of SOT by using MOKE microscopy.

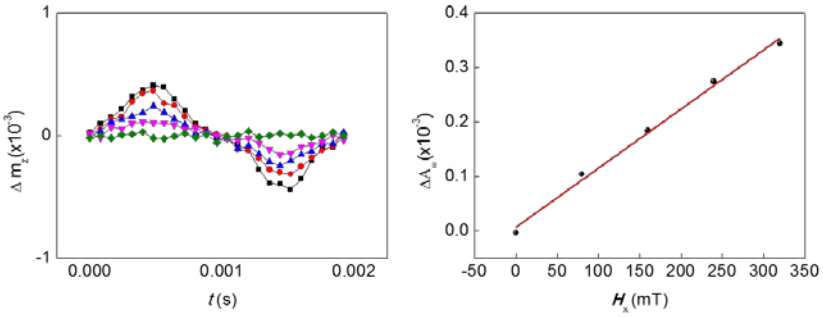

Figure 4.5 The SOT of Pt/Co/Mg/Pt structure longitudinal direction by using MOKE microscopy

4.2.3 Measurement technique of Dzyaloshinskii-Moriya interaction

The field driven DW motion with presence of DMI are observed in previous reports [19]. It is intensively studied in DW society in last few years due to its advantage in technological applications. The control of DW configuration is mostly engineering issue for high efficiency of spin torque device. From ref 19, the DMI field is measured by asymmetric DW expansion method. The in-plane field breaks the symmetry of radial direction of DW. The DMI field exist as internal in-plane field. We first observed circular DW by $+H_z$. Figure 4.6 shows up domain state as brighter regime. We then applied in-plane field $+H_x$ to this circular DW, which is expanded by moderate $+H_z$ pulse. Each expanded DW is successively monitored with respect to constant time interval pulse. For this study, Ta 5.0nm / Pt 2.5nm / Co 0.6 nm / X 5nm (X:

Ti(3d), Ru(4d), Pd(4d), Ta(5d), W(5d), Au(5d), and Mg) films with PMA are deposited on a Si substrate with 100 nm SiO_2 layer by dc-magnetron sputtering. The velocity of DW is observed by above method. The results are analyzed by creep equation with modified DW energy due to DMI in Section 4.2.4. Figure 4.6 illustrate the asymmetric DW expansion which determine the DW chirality.

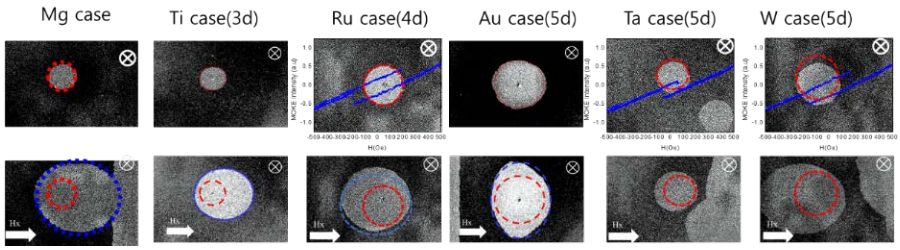

Figure 4.6 Asymmetric DW expansion of Pt/Co/X (X: Ti(3d), Ru(4d), Pd(4d), Ta(5d), W(5d), Au(5d), and Mg) films with PMA

4.2.4 Analysis of data of Dzyaloshinskii-Moriya interaction experiment

For the quantifying a DMI field $\boldsymbol{H}_{\mathrm{DMI}}$, the creep theory of DW determines a DW velocity using DW free energy[3, 27]. The DW free energy is given by

$$F(u,L) = \sigma_{DW}\frac{u^2}{L} - M_S HtLu \tag{4.10}$$

where first term is an elastic energy with DW energy density σ_{DW}, and the second term is Zeeman energy. The DW velocity is derived as follow

$$V = V_0 \exp\left[-\alpha(H_x)H_z^{-1/4}\right], \quad \alpha(H_x) \propto \left[\sigma_{DW}(H_x)\right]^{1/4} \tag{4.11}$$

The DW energy density σ_{DW} is generally affect the DW velocity. The σ_{DW} is generally considered as Bloch wall case, which has minimum magnetostatic energy. The DMI present case, however, is more proper for analyzing our experiment since DMI modified the DW energy density for chirality concerning. The DW energy density σ_{DW} are derived as follow [19],

$$\sigma_{DW} = \sigma_0 + 2K_D\lambda\cos^2\psi - \pi\lambda M_S(H_{DMI} + H_X)\cos\psi \tag{4.12}$$

Where ***D*** is DMI parameter, $\boldsymbol{K}_D$ is DW anisotropy energy, σ_0 is Bloch wall energy density, and λ is DW width. From this modified DW energy, we could determine a $\boldsymbol{H}_{\mathrm{DMI}}$ using asymmetric DW expansion experiment. The results are discussed in section 4.3.2.

4.3 Enhancement of SOT & DMI using Co PMA films with various transition metals

4.3.1 Enhancement of spin-orbit torque with 3d, 4d, 5d transition metals

Ta 5.0nm / Pt 2.5nm / Co 0.6 nm / X 5nm (X: Ti(3d), Ru(4d), Pd(4d), Ta(5d), W(5d), Au(5d), and Mg) films with PMA are examined for SOT measurement. The results are shown in figure 4.7. The longitudinal/transverse effective field are determined by electrical ω-2ω measurement method. We firstly are analyzed in longitudinal SOT (Field-Like SOT) for using a conventional spin Hall picture. Ta, Ti and W samples have enhanced SOT of 1052, 1294, 1041 Oe/10^{12}A/m^2 respectively, compared to ~200 Oe/10^{12}A/m^2 of Pt/Co/Pt structure. The Mg sample is unexpectedly large SOT of 5920 Oe/10^{12}A/m^2. In our strategy to enhance a SOT, seed/capping layer with different spin Hall sign, and larger spin Hall angle might increase a SOT as effective spin current increases.[5, 7, 8, 9, 11, 28~30]. The Ti and Mg case do not follow the spin Hall picture because they have relatively small spin Hall angle compared to Ta, W of 5d transition metals [30, 31].

We then analyzed in transverse SOT (Slonczewski-like SOT) for involving the Rashba picture. The Mg sample have a different sign of SOT in transverse geometry. This means the interfacial spin flip due to its hybridization of Mg and Co are opposite direction of other samples. Pd sample also have different sign, however, which magnitude of data is extremely small within the error bar. Ti sample has the largest SOT in transverse geometry. This might occur due to Ti oxidation. It could be compared with previous reports that heavy metal / ferromagnetic layer / oxide structure have same origin.

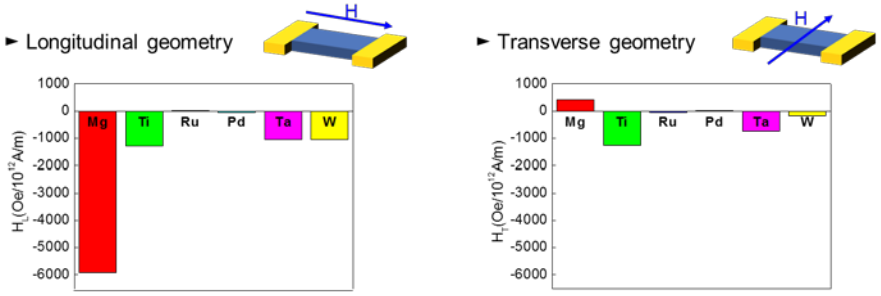

Figure 4.7 The result of SOT with electrical ω-2ω measurement method

4.3.2 Chiral structure of Co PMA films with presence of DMI

Ta 5.0nm / Pt 2.5nm / Co 0.6 nm / X 5nm (X: Ti(3d), Ru(4d), Pd(4d), Ta(5d), W(5d), Au(5d), and Mg) films with PMA are also investigated for DMI measurement. The results are shown in figure 4.8. This data described the DMI field $\boldsymbol{H}_{DMI}$ is enhanced maximum over 10 time of Pt/Co/Pt in previous report [32]. Most of the Pt/Co/X structure except for Pd case are the Néel wall structure when only H_z field is applied. For limitation of our in-plane magnet design, some of data is measured by angled expansion of DW. $\boldsymbol{H}_{DMI}\cdot\cos\theta$ are measured and then analyzed since small difference of DW velocity samples are generally hard to determine the $\boldsymbol{H}_{DMI}$. In our results, equilibrium state of the Néel wall structure are generated using material selection.

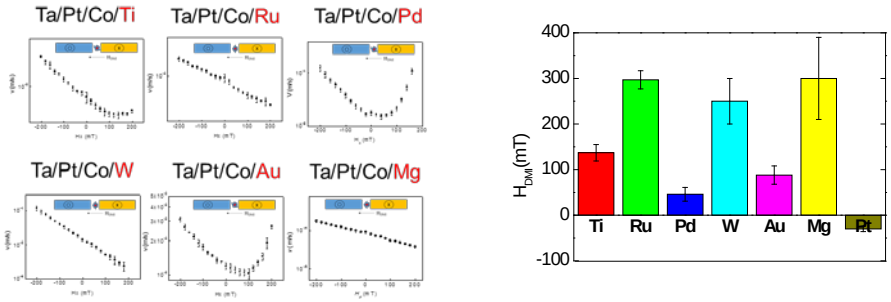

Figure. 4.8 The result of DMI using asymmetric DW expansion.

4.4 Material design rule for spin torque device

4.4.1 Introduction to schematic diagram for device engineering

Above the previous section, we report the SOT and DMI field of Ta/Pt/Co/X structure. The various functionality of spin torque memory device can be established by tailoring parameter. For instance, the SOT should be enhanced for fast DW motion and magnetization switching. The DMI should be controlled to determine a DW configuration to right-/left-handedness of rotating and homo-chiral Néel-type DW in ultra-thin films.

Here, the material table which contains SOT, DMI, Gilbert damping is organized for engineering device. Figure 4.9 shows schematic diagram of capping material tendency. The center of pentagon means generally bad performance. Gilbert damping constant give a high performance with small value. For the DMI field, Pt has a minus sign exceptionally. The spin Hall angle is from previous research [23]. The efficiency of spin torque increases as the thickness of ferromagnetic layer Co decreases.

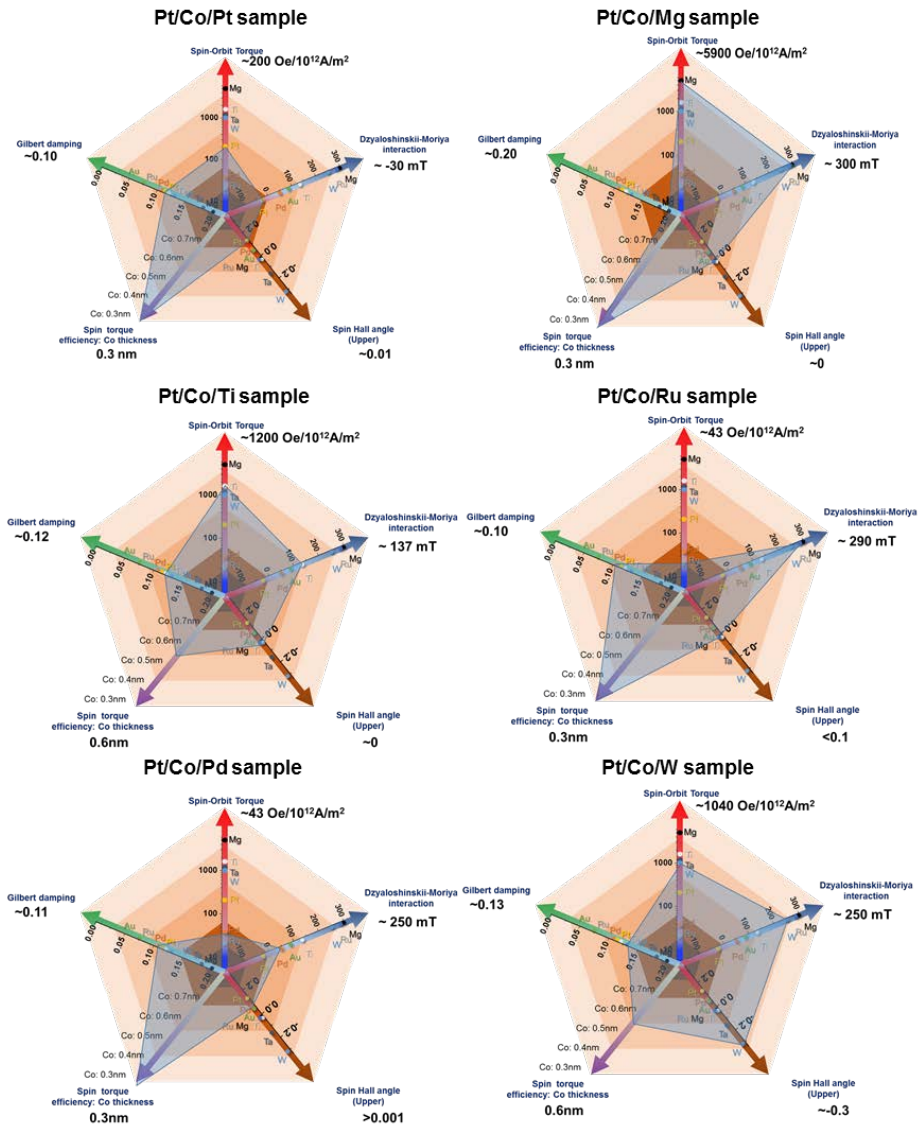

Figure 4.9 Pt/Co/X (X: Pt, Mg, Ti, W, Pd, Ru) schematic diagram material table.

The ideal material which cover a whole pentagon does not exist in our case. The SOT and DMI field have no correlation in our material table.

4.4.2 Potential applications of material design rule.

The schematics of material table give an implication to engineering a memory device. Each parameter of table have a relation with memory performance we already refer a chapter 1. The controlling of each parameter, for instance enhancement of SOT and sign control of DMI field, give a solution to applying a device. The details are discussed in next chapter.

Reference

[1] Slonczewski, J. C. *Phys. Rev. B* 39, 6995–7002 (1989).

[2] Slonczewski, J. C. *J. Magn. Magn. Mater*. 159, L1–L7 (1996).

[3] K.-J. Kim et al., *Nature* 458, 740 (2009).

[4] I. M. Miron et al, *Nature* 476, 189 (2011).

[5] Satoru Emori et al, *Nature Mat*. 12, 611(2013)

[6] A. Manchon and S. Zhang, *Phys. Rev. B* 79, 094422 (2009)

[7] Xin Fan et al, *Nature comm.* 5, 3042 (2014)

[8] K. Garello et al, *Nature nano.* 8, 587 (2013)

[9] Mahdi Jamali et al., *Phys.Rev.Lett.* 111, 246602 (2013)

[10] T. Tanaka. et al, *Phys. Rev. B* 77, 165117 (2008)

[11] Lugiao Liu. et al, *Phys.Rev.Lett.* 109, 096602 (2012)

[12] K.-W. Kim et al., *Phys. Rev. Lett*. 111, 216601 (2013)

[13] L. Liu et al., *Science* 336, 555 (2012)

[14] K-,W Kim et al,. *Phys. Rev. B* 80, 180404(R) (2012)

[15] S-,M Seo et al,. *Appl. Phys. Lett.* 101, 022405 (2012)

[16] T. Moriya, *Phys. Rev*. 120, 91 (1960)

[17] A. Fert et al. *Phys. Rev. Lett.* 44, 1538 (1980).

[18] S.-W. Jung et al. *Appl. Phys. Lett.* 92, 202508 (2008).

[19] S-.G. Je Ph.D. dissertation. Seoul National University (2015)

[20] J. Kim *Nature.Mat.* 12, 240(2013)

[21] Pi et al., *Appl. Phys.Lett.* 97, 162507 (2010)

[22] I. M. Miron et al., *Nature Mat* 9, 230 (2010)

[23] S. Maekawa, *Spin current*, oxford university press (2012)

[24] L. Liu, arXive 1111.3702 (2012)

[25] K.-W. Moon et al., Rev. Sci. Instrum., 80, 113904 (2009)

[26] S-.J. Yun, *Jour. Kor. Mag.Soc* 25(1), 1 (2015)

[27] J-.S. Ryu, *Phys.Rev.B* 84, 075469(2011)

[28] A. V. Khvalkovskiy, *Phys. Rev. B* 87, 020402(R) (2013)

[29] P. P. J. Haazen et al., Nature Mat. 12, 299 (2013)

[30] Chi-Feng Pai et al., *Appl. Phys.Lett* 101, 122404 (2012)

[31] S. Woo *Appl. Phys.Lett.* 105, 212404(2014)

[32] S-. G Je *Phys. Rev. B,* 88, 214401 (2014)

Chapter 5

DMI controlled by insertion layer

Previous chapter, we report the SOT and DMI field of various 3d, 4d, 5d transition metals and Mg capping samples with PMA. The material table based on this parameter have basic implications of designing a spin torque device. The each parameter have an intrinsic physical properties (i.e. electronic structure related on spin orbit coupling, crystal structure related on interface, magnetic properties related on spin dynamics) which means the basic application with material engineering method could be adapted. The interface control using inserting the layer are known as convenient method to control an electronic/magnetic properties originated by Fermi energy in recent research. [1,2].

In this chapter, we are controlling a DMI field by using inserting a high SOT materials into the Pt/Co/Pt structure. The film structure are Ta(5nm)/Pt(1.5nm)/Co(0.3)/Mg(t)/Pt which thickness of Mg varied from 0.3 nm to 1 nm. The DMI field are subtly observed by asymmetric DW wall expansions. The trend of Mg thickness dependence of DMI are discussed.

5.1 Introduction

The controlling of SOT and DMI have been intensively studied for spin torque memory device [1, 2, 4]. Recently, it is reported that the chirality originated by interfacial spin-orbit coupling makes the linear contribution term to LLG equation. It gives a possibility for engineering device. From the physical expectation of engineering interface, the SOT and DMI could be changed artificially. R. H. Liu et al.[4] reported that SOT is changed by induced voltage on samples. This voltage controlled an interfacial electric structure, which mainly modified a spin-orbit coupling state near Fermi energy. Gong Chen et al.[5] also reported that adjacent layer on ferromagnetic metal with different transition metal have a mainly changed DMI sign and its magnitude. The spin-orbit coupling strength are determined by electric outer shell of transition metals that made a hybridization of interface Co-transition metals.

In the previous chapter, the material dependence of SOT and DMI are reported for maximizing a spin torque efficiency. In material table with Pt/Co/X structure(X: Ti(3d), Ru(4d), Pd(4d), Ta(5d), W(5d), Au(5d), and Mg), the SOT and DMI are reported as intrinsic quantity related with its spin orbit coupling. This provide an engineering strategy which have been originated by band theory [3]. The SOT and DMI are known as spin orbit related phenomena. The Fermi energy are modified by interfacial coupling with strong spin orbit coupling materials. This mainly modified their interfacial orbital occupation and their hybridization. The interface modification on the Co layer, therefore, affect a Fermi energy that SOT and DMI can changed by interfacial spin orbit coupling.

In this chapter, we focused on the method based on spin torque

material table to control SOT and DMI. The Figure 5.1 illustrate the SOT and DMI of Pt and Mg sample.

The high SOT adjacent material, i.e. Mg, is almost 30 times larger than original Pt case (Pt/Co/Pt ~ 200 [Oe/10^{12}A/m^2]). The DMI sign of Mg, however, is different with Pt case (Pt: -30 ± 3mT, Mg: 300 ± 80mT). The enhancement of SOT and DMI sign change will be discussed in next section by using interface engineering.

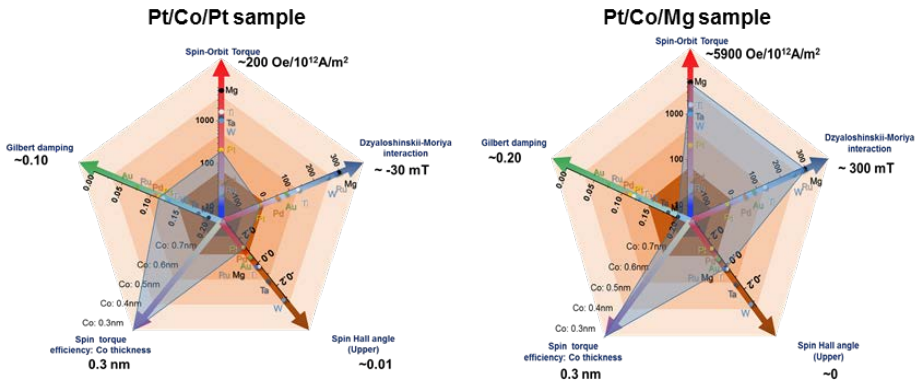

Figure 5.1. Pt/Co/Pt and Pt/Co/Mg sample schematic material table.

5.2 Controlling of DMI field by Mg insertion layer

The DMI field, $\boldsymbol{H}_{\mathrm{DMI}}$ are introduced as internal field of DW configuration which determined a DW motion direction and spin torque efficiency. Spin current due to Pt layer or other adjacent metals are determined by its intrinsic spin Hall angle [10~12]. It is, therefore, spin current direction is deterministic state when the adjacent metal was chosen. For instance, the Pt under layer generate the spin current direction to DW moving along the current

direction [13]. When the current is injected to the sample with the DMI field, the magnetization switching prefer the direction which maximized SOT efficiency [14].

From the previous material result, adjacent Mg layer is reported to have a large DMI field and a different DMI sign with Pt layer. The upper Pt layer is source of opposite spin current to its bottom Pt layer. It could be reduced the effective spin current. The Mg layer insertion, however, prevent a spin current from upper Pt layer. The Co-Pt interface could be modified using Mg insertion with monolayer level control. The Co-Mg interface have a different DMI field sign compare to the Co-Pt interface, which Mg insertion layer could be change the DMI field sign gradually. In the microstructural aspect, we deposit Mg layer by using sputtering with polycrystalline state. The monolayer control of Mg insertion means the interface composition of Mg will be increased until continuous film state. This gradual increasing of Co-Mg bonding modify a spin-orbit coupling of Co-Pt state [3]. The spin-orbit coupling of Co-Mg have different spin hopping preference, which $\boldsymbol{H}_{\mathrm{DMI}}^{\mathrm{eff}}$ could be derived as following equation,

$$H_{DMI}^{eff} = H_{DMI}^{Pt} + \alpha H_{DMI}^{Mg} \tag{5.1}$$

The α is coefficient related with Mg thickness. We determine the $\boldsymbol{H}_{\mathrm{DMI}}^{\mathrm{eff}}$ using asymmetric DW expansion method [14]. The sample structure are Ta 5nm / Pt 1.5 nm / Co 0.3 nm / Mg t nm /Pt 2 nm with t = 0.3, 0.5, 0.7, 0.9, 1.0 nm. The base pressure is under 1.0×10^{-8} torr for preventing oxidation. The pre-sputtering condition of Mg is 100W with 1 min with RF condition. The Ar

purity are used 99.9999%. The deposition time of Mg is under 10sec for preventing deposit oxidation. This sample shown a clear circular DW. [Figure 5.2]

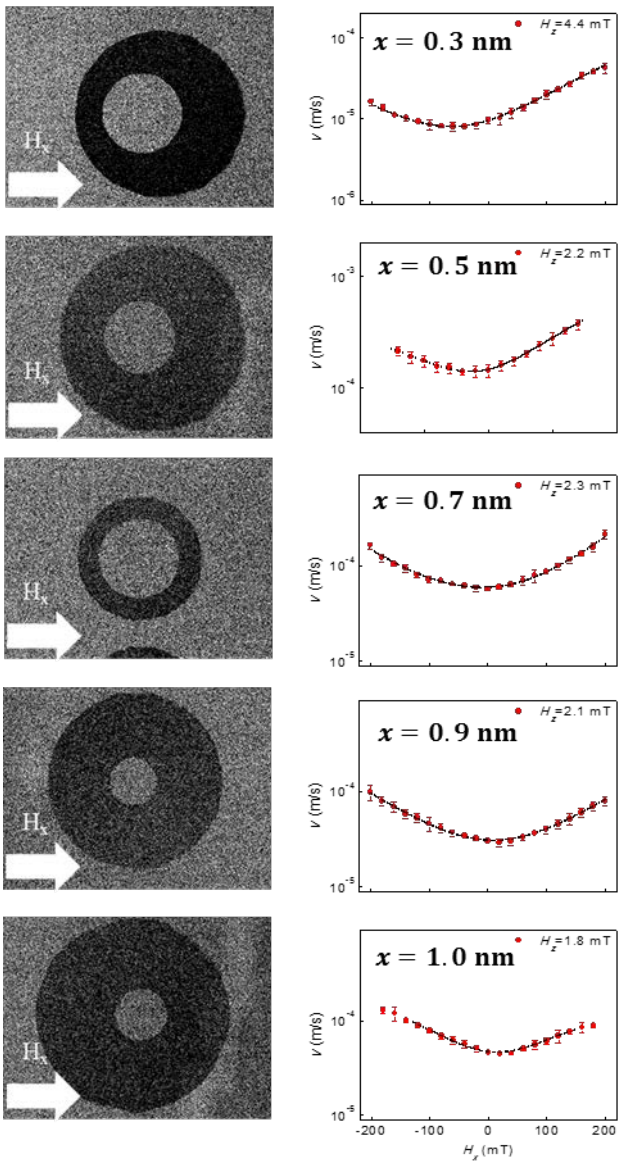

Figure 5.2. The light-gray DW images are initial DW state. The dark-gray DW images are final DW state with respect to a same in plane field direction. The DMI field curve move a gradually

The asymmetric DW expansion results are shown in figure 5.3. The DMI field are gradually decreased with increasing Mg thickness. This results perfectly match with our expectation. The thickness of Mg insertion about 0.8 nm sample have zero DMI field. This means the chirality of DW is changed, which the sample have perfect Bloch wall state. The artificial Bloch wall attracts great interest since the Walker-Breakdown would be exist. For the technical aspect, the precisely controlled DMI with different sign could be applied in spin torque device. The direction of DW motion and controlling of spin torque efficiency are radical design rule for tailoring a spin torque memories. By using our material table, the tailored film are generated which enhance a density and read-write reliability of spin torque device in the epi-level.

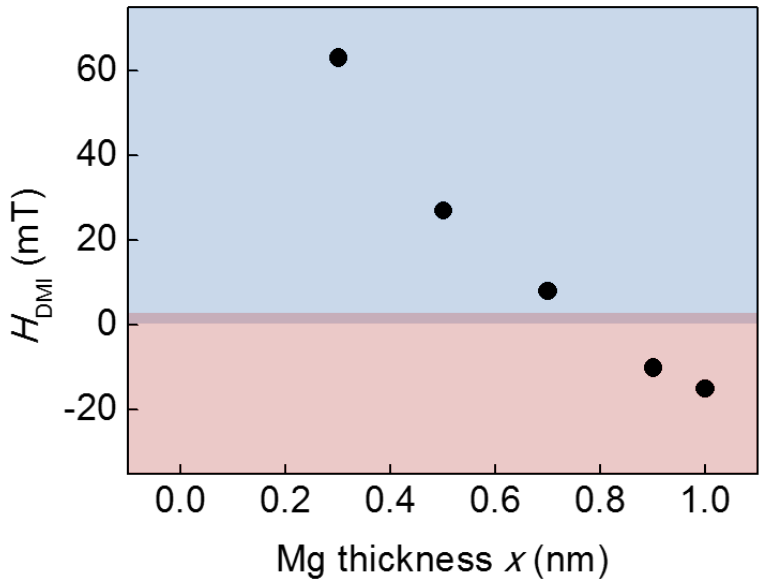

Figure 5.3 DMI field, $H_{DMI,}$ changes gradually due to top-interface variation.

5.3 Enhancement of SOT by Mg insertion layer

Most Co-adjacent materials in PMA sample have a large SOT and DMI. This made the interfacial anisotropy that could be originated by spin orbit coupling between Co and adjacent material [7]. The Fermi energy, modified by interfacial electronic structure, make the changing of SOT and DMI [3, 8]. For this study, we basically changed the Fermi energy by using interface modification [18, 19]. The material insertion or doping method are well known as modification of Fermi energy. In Co PMA system, the Fermi energy level are generally understood with hybridization of s-d spin-orbit coupling on interface of Co layers [7, 8]. The insertion of Mg layer which have extremely small spin-orbit coupling strength directly changes this s-d coupling

state. This could be explained by the SOT based on spin Hall picture. The Co-Mg interface with changed s-d coupling state is expected to block spin current from upper Pt layer, or enhance the spin current because Co-Mg or Mg-Pt interface has opposite spin Hall angle to bottom Pt layer. The effective spin current of DW motions are totally increased when the Mg insertion layer exist. This is almost same SOT mechanism of heavy metal / ferromagnet /oxide heterostructure. The Pt/Co/Mg/Pt structure have also structural inversion asymmetry, which means the Rashba picture could be possible to explain of boosting SOTs. The total scenarios are be discussed in section 5.4.

The electronic structure of neighboring atoms affect a magnitude and sign of DMI field and the DMI field generally affected the hopping sequence through neighboring atoms. The inserting Mg layer on Pt/Co/Pt structure is this case. Many of transition metal have a same DMI field sign with Pt/Co/Mg structure when deposited on Pt/Co. The Pt/Co/Pt structure are exceptionally, however, different sign of DMI in our study. The spin-orbit coupling state between Co/Pt could be modified by Mg inserting layer. These gives an implication, therefore, that we could control a spin-orbit coupling with inserting layer which have different DMI sign.

Figure 5.3 illustrate a ω-2ω measurement by MOKE microscopy. This is for eliminating an artifact of electric signal, such as planar Hall effect, anomalous Nernst effect [9]. *S.-J. Yun et. al* report the analysis of this signal use of circular polarized polar MOKE [16]. The measurement component of transverse and longitudinal of the SOT are quantified. This alternative way of measurement give a precise quantity for cross-checking with previous results of electric-measurement. Fig 5.2 (a) show the $\sin\omega t$ with different H_x. Each H_y is fixed. The field of anisotropy with Pt/Co/Mg(1)/Pt sample have 2T±21mT using extraordinary Hall torque measurement.[17] From the equation 4.9, the

longitudinal SOT H_L is about 4000 Oe/10^{12}A/m, the transverse SOT H_T is almost 0 Oe/10^{12}A/m. This enhancement of SOT means also explained by spin Hall picture due to bottom spin current of Pt layer. The Mg layer with hybridization of Co-Mg or capping Mg-Pt could have different spin Hall angle comparing to bottom Pt layer. Or other possible explain is upper Mg prevent a spin current from upper Pt layer. This should be careful analysis with structural aspect for future research.

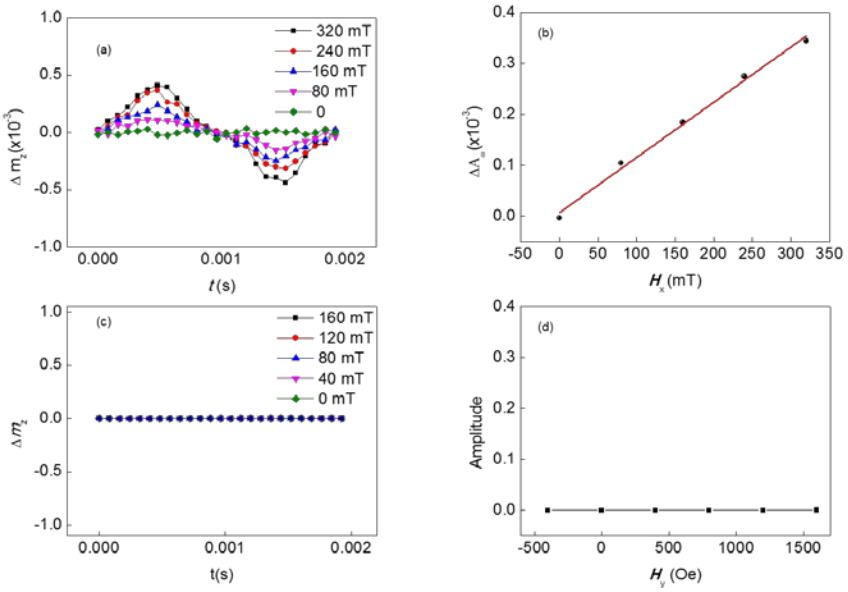

Figure 5.3 SOT ω-2ω measurement by MOKE microscopy. (a), (b) longitudinal SOT with respect to various H_x. (c), (d) transverse SOT with respect to various H_y

5.4 Discussion

Controlling DMI field and enhancement of SOT is well engineered by Mg insertion on Pt/Co/Pt structure. The Mg thickness of 1 nm make a drastic change of SOT. This enhancement of SOT need precise analysis because Mg is easy to be MgO. In MgO case, Co-O bonding could also modifying this enhancement. To avoid oxidation of Mg layer, we use following conditions during deposition. The Mg layer are metallic state when the base pressure~10^{-9}torr, Ar purity 99.9999%, pre-sputter with RF power 200W(<1min), and deposition time Mg under 10sec. For the confirming a metallic Mg, we should check a structural analysis with XPS, TEM, and etc. The total band structure, furthermore, should be calculated for understanding this phenomena.

Reference

[1] A. Hrabec et. al., *Phys. Rev. B* 90, 020402(R) (2014)

[2] Minh-Hai Nguyen et al., *Appl. Phys. Lett*. 106, 222402 (2015)

[3] Private discussion with Prof. K.-J. Lee, The conventional theory of SOT and DMI can exactly explained by its band calculation. The spin Hall and Rashba picture are general asymptotic equation of actual band that the engineering an interface are implied a modification of Fermi energy.

[4] R. H. Liu et al., *Phys. Rev. B* 89, 220409(R) (2014)

[5] K.-W Kim et al., *Phys. Rev. Lett*. 111, 216601 (2013)

[6] Gong Chen, et al., *Appl. Phys. Lett.* 106, 062402 (2015)

[7] P. Bruno et al, *Phys. Rev. B* 39, 865 (1989)

[8] N. Nakajima et al. *Phys. Rev. Lett*. 81, 5229 (1998)

[9] K. Garello et al, *Nature nano.* 8, 587 (2013)

[10] Axel Hoffman *IEEE Trans. Mag*., 49 (10), (2013)

[11] Chi-Feng Pai et al., *Appl. Phys. Lett* 101, 122404 (2012)

[12] T. Tanaka et al., *Phys. Rev. B* 77, 165117(2008)

[13] J.-C. Lee et al., *Phys. Rev. Lett.* 107, 067201 (2011)

[14] I. Miron et al., *Nature,* 467, 189 (2011)

[15] S-. G Je *Phys. Rev. B,* 88, 214401 (2014)

[16] S-.J. Yun et al., *Jour. Kor. Mag. Soc* 25(1), 1 (2015)

[17] K.-W. Moon et al., *Rev. Sci. Instrum.*, 80, 113904 (2009)

[18] Z. Bryan et al., *J. Electron Mater,* 42(5), 815 (2013)

[19] R. Shan et al., *Phys. Rev. Lett.* 102, 246601(2009)

Chapter 6

Conclusion and outlook

In this study, we investigated physical origin of spin torque device. The Gilbert damping, mainly related on DW velocity and low energy consumption, are controlled by empirical relation with coercive field. For enhancement of SOT which related on read/write reliability, we manufactured several PMA films by sandwiching Co with 3d, 4d, or 5d transition metals. We also reported the boosting of SOT that cannot be explained with former theories of Rashba or spin Hall picture. The DMI field which related on high-density and skyrmion dynamics are reported on various transition metals interface. The material table including this results are organized for engineering device. The Mg insertion as a high SOT generating capping layer chosen for controlling a DMI and enhancement SOT. The DMI field is experimentally controlled for high SOT material based on material design rule. The precise structural analysis are needed in future work.

These results discussed above imply that the spin torque devices have advantages such as high-density, low energy consumption and read/write reliability compared to the other memory devices. We can conclude, therefore, the spin torque devices are very promising one for the next generation memory. This hierarchical approach to tailor spin torque memory devices is becoming a stepping stone to the future of nanomagnetism.

Appendix

Appendix A

Landau-Liftshitz-Gilbert equation in presence of the current induced torque

$\frac{\partial \hat{m}}{\partial t} = -\gamma \hat{m} \times \left(\vec{H}_{ext} + \vec{H}_{ani}\right) + \alpha \hat{m} \times \frac{\partial \hat{m}}{\partial t} - \gamma H_T(\hat{m} \times \hat{y}) + \gamma H_L(\hat{m} \times (\hat{m} \times \hat{y})$

$\widehat{m}$: Magnetization unit vector

γ: gyromagnetic ratio

$H_{L,T}$: effective longitudinal/transverse magnetic field

$\vec{H} = H_x\hat{x} + H_y\hat{y} + H_z\hat{z}$ in spherical coordinate

$\vec{H} = H_x \sin\theta \cos\varphi\, \hat{r} + H_x \cos\theta \cos\varphi\, \hat{\theta} - H_x \sin\varphi\, \hat{\varphi}$

$+H_y \sin\theta \sin\varphi\, \hat{r} + H_y \cos\theta \sin\varphi\, \hat{\theta} - H_y \cos\varphi\, \hat{\varphi}$

$+H_Z \cos\theta\, \hat{r} - H_Z \sin\theta\, \hat{\theta}$

$H_{ani} = H_k m_z \hat{z} = H_k m \cos\theta \left(\cos\theta \hat{r} - \sin\theta\, \hat{\theta}\right) = H_k m \cos^2\theta\, \hat{r} -$

$H_k m \cos\theta \sin\theta\, \hat{\theta}$

For an equilibrium state $\frac{\partial \hat{\mathrm{m}}}{\partial t} = 0,\ |\mathrm{m}| = 1$

$-\gamma\ \times \vec{\mathrm{m}} \times \left(\vec{H}_{\mathrm{ext}} + \vec{H}_{\mathrm{ani}}\right) = -\gamma\ \times \hat{m} \times \left(\hat{H}_{ext} + \hat{H}_{ani}\right) = -\gamma \times$

$[(H_x cos\theta cos\phi + H_y cos\theta sin\phi - H_z sin\theta)\hat{\phi} - \left(-H_x sin\phi + H_y cos\phi\right)\hat{\theta} -$

$H_k cos\theta sin\theta\hat{\phi}]$

$\hat{\mathrm{m}} \times \hat{\mathrm{y}} = \cos\theta\sin\phi\hat{\phi} - cos\phi\hat{\theta}$

$\hat{\mathrm{m}} \times \hat{\mathrm{m}} \times \hat{\mathrm{y}} = \cos\theta\sin\phi\left(-\hat{\theta}\right) - \cos\phi\hat{\phi}$

$\hat{\theta}: \mathrm{H_x}\sin\phi - \mathrm{H_y}\cos\phi - \mathrm{H_T}\cos\phi + \mathrm{H_L}\cos\theta\sin\phi = 0$

$\hat{\phi}: (\mathrm{H_x}\cos\phi + \mathrm{H_L})\cos\phi + \left(\mathrm{H_T} + \mathrm{H_y}\right)\cos\theta\sin\phi - (\mathrm{Hz} + \mathrm{H_k}\cos\theta)\sin\theta = 0$

i) Case 1. $\theta \approx 0°$

$\cot\phi = \frac{\mathrm{H_x}+\mathrm{H_L}\cos\theta}{\mathrm{H_y}+\mathrm{H_T}}$, $(\sin\phi = \frac{\mathrm{H_y}+\mathrm{H_T}}{\sqrt{(\mathrm{H_x}+\mathrm{H_L}\cos\theta)^2+\left(\mathrm{H_y}+\mathrm{H_T}\right)}}, \cos\phi =$

$\frac{\mathrm{H_x}+\mathrm{H_L}\cos\theta}{\sqrt{(\mathrm{H_x}+\mathrm{H_L}\cos\theta)^2+\left(\mathrm{H_y}+\mathrm{H_T}\right)}})$

$(\mathrm{H_z} + \mathrm{H_k}\cos\theta)\sin\theta = \frac{\left(\mathrm{H_y}+\mathrm{H_T}\right)^2\cos\theta+(\mathrm{H_x}\cos\theta+\mathrm{H_L})(\mathrm{H_x}+\mathrm{H_L}\cos\theta)}{\sqrt{(\mathrm{H_x}+\mathrm{H_L}\cos\theta)^2+\left(\mathrm{H_y}+\mathrm{H_T}\right)^2}}$

Using taylor expension $\cos\theta\sim1, \sin\theta\sim\theta\ \ O(\theta^2)\sim0$

$(\mathrm{H_z} + \mathrm{H_k})\theta = \sqrt{(\mathrm{H_x} + \mathrm{H_L})^2 + \ \left(\mathrm{H_y} + \mathrm{H_T}\right)^2}$

ii) Case 2. $\theta \approx 90°$

For θ is almost perpendicular to y axis, so cosθ~sinθ, sinθ~cosθ

Hence above equation will be reduce as

$\hat{\theta}: H_x \sin\phi - H_y \cos\phi - H_T \cos\phi + H_L \sin\theta \sin\phi = 0$

$\hat{\phi}: (H_x \cos\phi + H_L)\cos\phi + (H_T + H_y)\sin\theta \sin\phi - (Hz + H_k \sin\theta)\cos\theta = 0$

Using taylor expension $\cos\theta \sim 1, \sin\theta \sim \theta$

$\theta = \frac{H_y + H_T}{H_x + H_L} \tan\phi,$

$(H_x \cos\phi + H_L)\cos\phi + [(H_T + H_y)\sin\phi - H_k]\theta - Hz = 0$

$\theta = \frac{[(H_x \cos\phi + H_L)\cos\phi - Hz]}{[H_k - (H_T + H_y)\sin\phi]}$

Author's Biography

Cheong-Gu Cho

Personal Information

(Citizenship) South Korea (Birth) Aug. 15th, 1984 (Gender) Male (Marital Status) Single (Contact) 02-884-9254 (Cell) 010-9666-3129 (Home) 02-780-1129 (E-mail) jogufs@snu.ac.kr

Research Interest

- **Spintronics:** Sample nano-fabrication, Material research and Electric/Optical measurement
- **Interdimensional university and critical phenomena** in physical, 1D & 2D system
- **Spin Orbit torque:** spin torque by asymmetric sample structure or by spin current due to spin Hall effect
- **Dzyaloshinskii-Moria interaction:** Chiral spin structure within the spin torque device
- **Fast Demagnetization phenomena** in magnetization dynamics
- General Condensed-matter Physics and General physics, Femto-second level phenomena

Academic Training

Mar.2010 ~ present	Ph.D. Candidate(ABD) In Physics, Seoul National University ▪ 1 semester of Laser physics graduate courses ▪ 1 semester of graduate advanced laboratory courses [AFM manufacture] ▪ Manufacturing a sputter system with ultra-high vacuum ▪ Research with Prof. Choe using MOKE(Magneto-Optical Kerr effect)
Mar. 2008 ~ Feb. 2010	M. S. In Physics at Seoul National University ▪ 2 semesters of electrodynamics graduate courses ▪ Many Other physics courses (including Quntum mechancis)

Mar. 2004 ~ Feb. 2008	B. S. In Physics at Chung-Ang university ▪ minor : Mathematics ▪ 2 semesters of Optics undergraduate courses ▪ Graduate paper : Optical properties of CNT using Raman spectroscopy

Honors and Scholarships

Fall. 2004	Tuition Scholarship from CAU
'04, '06, '07	Award of most reading person in CAU (Natural science section)
Fall 2005	CAU Culture challenger : Best team award (Year of Physics, Beyond Einstein Conference in EPS)
Fall 2006	Best poster award from Korean Physical Society (Comic ray detector-MWPC)
Fall 2007	Honor of Yeongdengpo-gu citizen
Fall 2009	Best poster award from Korean Physical Society (Measurement of perpendicular magnetic anisotropy in ultra-thin films : Extraordinary hall torque measurement)
Fall. 2011 ~	Hi-Seoul Scholarship
Fall 2012	Best tutor in department of physics of SNU [Course of modern physics experiment(Intermediate level)]

Publications

1. **Cheong-Gu Cho**, Joon Moon, Sang-Jun Yun, Hyun-Seok Whang, Dae-yeon Kim, Soong-Geun Je, and Sug-Bong Choe “Enhancement of spin-orbit torque and Dzyaloshinskii-Moriya interaction in Co films sandwiched by various 3d, 4d, and 5d transition metals” Manuscript will be prepared.
2. **Cheong-Gu Cho**, Joon Moon, Joo Sung Kim and Sug-Bong Choe, Cheol-Hyun Moon and Byoung-Chul Min, Sang-Il Kim and Seung-Young Park“Optimization of the Gilbert damping constant by annealing CoFeB films sandwiched by Ta, Ru, and Pd layers” J.Kor.Phys.Soc.65(10), 1161(2014)
3. Sang-Jun Yun, **Cheong-Gu Cho**, Sug-Bong Choe“ Simultaneous excitation of two different spinwave modes by optical ultrafast demagnetization” Appl. Phys. Express submitted(2015)
4. Duck-Ho Kim, Sang-Cheol Yoo, Dae-Yun Kim, Kyoung-Woong Moon, Soong-Geun Je, **Cheong-Gu Cho**, Byoung-Chul Min, and Sug-Bong Choe “Maximizing domain-wall speed via magnetic anisotropy adjustment in Pt/Co/Pt films” Appl.Phys.Lett. 104, 142410(2014)
5. Sung-Min Ahn, Kyoung-Woong Moon, **Cheong-Gu Cho**, Sug-Bong Choe “Control of Domain-Wall Injection Field with Different Nucleation Pad Geometry” J.Nanosci.Nanotechnol.11(7), 6476(2012)
6. Sung-Min Ahn, Kyoung-Woong Moon, **Cheong-Gu Cho** and Sug-Bong Choe “Control of domain wall pinning in ferromagnetic nanowires by magnetic stray fields” Nanotechnology 22, 025702(2011)
7. Jae-Chul Lee, Kang-Soo Lee, **Cheong-Gu Cho**, Kyoung-Woong Moon, Kyung-Ho Shin, and Sug-Bong Choe “Domain Patterns and Magnetization Reversal Behaviors in Oxide/Co/Pt Films” IEEE Trnas. Magn. 46, 2009(2010)

Research Experience

Feb. 2009~ Present.	**THz Magnetic Nano-device LAB**
	Nanostructure sample fabrication & Optical measurement(MOKE)
	Electrical measurement of Domain wall deviece
	Ultra Hig vacuum sputter system manufacturing
	Lithography with photo/e-beam
	XRD/XRR technique
Jan. 2006~ Feb. 2008	**Nanostructure spectroscopy LAB**
	Optical properties of CNT using Raman spectroscopy
	Optical properties of GaAs, indirect Semiconductor using Photoluminesence

Aug. 2005~ Sep. 2006	**Cosmic ray detector Group study** Worked in Multi-wire propotional chamber setting Simulation of muon detection & electric field calculation
Jul. 2005	**Year of Physics : Beyond Einstein conference** CAU Culture challenger : Undergraduate school student forum

Miscellaneous

Program skills	▪ C, Labview ▪ Mathematica, MatLab ▪ MS WORD, Excel, Power point,
Military Service	▪ Technical Research Personnel

국문 초록

현재 사용되는 DRAM의 회로 선폭이 물리적 한계에 근접한 10 nm 대역으로 내려감에 따라 생산 비용이나 구조화 등에서 여러 문제가 발생하기 때문에, 이를 극복하기 위하여 차세대 메모리 소자에 대한 관심이 계속하여 증가하고 있다. 이 중에서도 스핀토크 현상을 이용한 자성메모리는 읽기/쓰기 시간, 내구성, 비휘발성, 전력 소모 등에서 경쟁력을 확보하여 학문적 측면뿐 아니라 산업적으로도 연구가치가 대두되었다.

이 논문은 자성메모리 소자 중 대표적인 스핀토크 소자(Spin torque device)가 양산하기 위해 해결해야 하는 물리적인 문제들에 대해 연구를 진행하였다. 스핀토크 소자가 차세대 메모리로 사용되기 위해 갖춰야 하는 가장 큰 물리적인 한계는 **1)High speed, 2)Read-Write reliability, 3)High density & low energy consumption** 이며, 메모리 성능을 향상시키는 것과 더불어 새로운 물리적인 상황을 발견하고 해결하는 과정을 담았다.

Chapter 1에서는 spin을 이용한 새로운 memory의 등장과 spin torque소자의 전망에 관하여 소개하려고 한다. 최근 다양한 종류의 차세대 메모리가 등장함과 함께 spin을 이용한 memory만이 갖는 특징에 대해서 설명할 것이다. 현재 스핀 토크를 이용한 소자는 크게 두 가지 방향으로 연구가 진행되고 있다. 먼저 나노기둥 모양의 비자성층에 의해 분리된 두 자성층의 자화방향을 전류로 제어하며 메모리 역할을 수행하게 하는 STT-MRAM에 대해 소개하고, 다음으로 나노선 안에 여러 개의 자구벽을 형성시켜 이를 스핀 전류를 구동시키는 자구벽 메모리에 대해 소개하려고 한다.

Chapter 2에서는 자성메모리 소자를 구현하기 위하여 증착과정에서 생기는 결함에 의해 자구벽의 이동영향을 최소화시킨 수직 자성초박막을 구현하는 방법에 대한 연구결과를 보고하고자 한다. 이를 위해 박사과정 동안 완성한 Sputtering system을 이용하여 다양

한 다층박막 소자의 제작방법을 소개한다. 또한 박막의 흠결과 두께에 대한 정확성을 측정하기 위하여 XRD/AFM을 이용하여 초박막의 구조적인 특성을 분석한다. Chapter 3, 4, 5에서 연구에 사용될 박막의 특징에 관해 간략히 소개하고자 한다.

Chapter 3에서는 스핀 토크소자의 High performance와 관련된 Gilbert damping constant에 관한 연구에 관해 보고하고자 한다. 먼저 Gilbert damping에 대한 물리적인 소개와 이를 연구하는 것이 소자 특성에 중요한 이유에 대해 설명하려고 한다. 이 chapter는 Gilbert damping constant를 Optimize하는 방법을 연구를 목표로 진행하였다. Gilbert damping constant를 변화시키는 다양한 자성특성에 대해 관찰하였고, 이를 구조(structure)적인 변화를 통해 control할 수 있는 방법을 보고 하였다.

Chapter 4에서는 수직자성초박막에서 최근 발견된 Spin-orbit torque와 Dzaloshinskii-Moriya interaction에 관한 연구결과를 보고하고자 한다. Spin torque 소자의 양산에 중요한 Read-Write reliability, High density & low energy consumption 문제 해결에, SOT와 DMI의 역할에 대해 소개한다. 또한 이를 통해 spin torque 소자에 적합한 최적 구조의 수직자성초박막을 보고하고, material design rule에 관해 논하도록 한다.

Chapter 5에서는 Chapter 4에서 논의한 물질특성을 이용하여, SOT의 향상과 DMI field의 실제적 조절실험에 관하여 보고하도록 하겠다. 이를 위해 Mg층의 삽입을 통한 물리적 현상의 변화에 관하여 논하도록 한다.

Chapter 6에서는 Thesis의 연구 결과에 대해 논하도록 하겠다. 새롭게 발견한 SOT와 DMI의 결과를 통해 spin torque 소자의 양산에 이점에 관해 설명하고, 물리적 의의에 관해 보고하려고 한다.